https://doi.org/10.5194/egusphere-2024-1746
Preprint. Discussion started: 20 August 2024

Geomorphic analysis and fluvial incision rates from valley-filling lava flows: implications for the Quaternary morphotectonic evolution in the Moroccan Massif Central and Middle Atlas

Ahmed Yaaqoub[1], Abderrahim Essaifi[1], Romano Clementucci[2,3], Paolo Ballato[2], Rachid Zayane[1], Claudio Faccenna[2], Carolina Pagli[4]

[1]Département de Géologie, FSSM, B.P. 2390, Université Cadi Ayyad, Marrakech, Maroc.

[2]Dipartimento di Scienze, Università degli studi Roma Tre, Roma, Italia.

[3]Department of Earth Sciences, ETH Zurich, Zurich, Switzerland

[4]Dipartimento di Scienze della Terra, Università di Pisa, Pisa, Italia.

*Correspondence to: Ahmed Yaaqoub (*ahmed.yaaqoub@ced.uca.ma)

Abstract

Fluvial dynamics is one of the main surface processes that shape the Earth's topography. Geomorphic records, such as fluvial terraces, play a crucial role in reconstructing the history of landscapes and deciphering the complex interactions among tectonic activity, lithology, and surface processes, which are primarily controlled by climate. This is also valid in valleys characterized by the emplacement of effusive volcanic rocks that are generally more resistant to erosion, and hence have a high preservation potential, and are easier to date than alluvial deposits. Valley-filling volcanic rocks, thus, represent ideal geomorphic

https://doi.org/10.5194/egusphere-2024-1746
Preprint. Discussion started: 20 August 2024

markers to estimate the magnitude and the spatio-temporal pattern of fluvial incision and associated forcing mechanisms.

In this study, we combine fluvial incision rates on dated lava flows emplaced in the valleys of the Moroccan Massif Central and Middle Atlas with DEM-based geomorphic analysis to gain insights into the Quaternary landscape evolution. The results show that incision rates are in the order of 0.01 and 0.1 mm yr^{-1} for the Middle Atlas and the Massif Central respectively. This spatial discrepancy in incision rates agrees with geomorphic metrics, with lower rates within the low topographic relief landscape and higher rates (up to one order of magnitude) along its margins that are highly dissected by fluvial incision. The comparison between our data and published incision rates in the northeastern flank of the Middle Atlas suggests that the eastern flank of the Middle Atlas accommodates active tectonic shortening. Furthermore, our analysis indicates that lithology and climate may not be the primary factors controlling the observed spatial variation in incision rates between the Middle Atlas and the Massif Central. Instead, surface uplift, which is probably related to forebulge flexural uplift enhanced by dynamic mantle-related uplift, could have triggered relatively high incision rates in the Massif Central. Ultimately, we conclude that a significant proportion of the topographic relief in our study area has been generated before the lava emplacement (i.e., earlier than 2.85 Ma).

Keywords: Incision rates, lava flows, Middle Atlas, Massif Central, Morphotectonic evolution, Quaternary

1. Introduction

The evolution of the Earth´s landscapes is the product of the perpetual interactions between tectonics, which tend to construct topography through rock uplift, and surface processes, which work to reshape and lower it (e.g., Ahnert, 1970; Kirby and Whipple, 2012; Whipple and Tucker, 1999; Whittaker,

https://doi.org/10.5194/egusphere-2024-1746
Preprint. Discussion started: 20 August 2024

2012; Wobus et al., 2006). Fluvial incision is one of the most important geological exogenic process that drives the evolution of landscapes. Therefore, quantifying fluvial incision rates is pivotal in understanding the pace and patterns of landscape development (Wolff et al., 2018). Bedrock rivers are sensitive to changes in boundary conditions such as uplift, rock erodibility, base-level elevation, and climate, and bedrock rivers communicate base-level changes to the whole catchment, dictating the pattern of erosion and deposition (Boulton, 2020; Lanari et al., 2020; Whipple et al., 2013). As such, fluvial landforms constitute archives that encode valuable information about tectonic and climatic conditions of a given region (Demoulin et al., 2017; Evenstar et al., 2020). With the advent of Quaternary geochronology, fluvial terraces are increasingly used to quantify incision and uplift rates and to infer tectonic and climatic histories (Agharroud et al., 2021; Burbank and Anderson, 2011; Fuller et al., 2009; Lavé and Avouac, 2001; Pastor et al., 2015; Pazzaglia, 2013). Similarly, many volcanic terrains provide good location to measure incision and denudation rates (Clementucci et al., 2022; Ott et al., 2018). Fluid lava flows emplaced along the preexisting valleys create an isochronous surface. The post-emplacement undercutting by fluvial incision and the formation of fluvial strath terraces provides the possibility to quantify rates of erosion/incision. Many studies took advantage of this interaction river-lava to quantify fluvial incision rates and constrain landscape evolution (e.g., (Allen et al., 2011; Bridgland and Westaway, 2014; Demir et al., 2007; Ott et al., 2018; Schildgen et al., 2007).

The Middle Atlas Mountains is the northeast branch of the Atlas system of Morocco. It is a Cenozoic intracontinental belt that resulted from the inversion of an aborted Triassic-Jurassic rift that affected the Hercynian terrains of the Moroccan Meseta (Charrière, 1990; Mattauer et al., 1977; Michard, 1976). The polyphased tectonogenesis of the Middle Atlas, is related to the Africa-Europe convergence, and took place in the Neogene before the late Miocene and during the Pliocene (Charrière, 1984, 1990). Tectonic shortening, however, is too moderate to solely account for the high elevation of the belt (Arboleya et al., 2004; Gomez et al., 1998). A long-wavelength mantle-driven uplift is thought to have contributed to the generation of high topography as also suggested for other mountain belts of Morocco (e.g., Babault et al., 2008a; Clementucci et al., 2023a, b; Frizon de Lamotte et al., 2009; Lanari et al., 2023b; Miller and Becker,

https://doi.org/10.5194/egusphere-2024-1746
Preprint. Discussion started: 20 August 2024

2014; Missenard et al., 2006). This interpretation is supported by the occurrence of a thinned mantle lithosphere associated with scattered alkaline volcanism that stretches from the Siroua Massif in the Anti-Atlas towards the Mediterranean sea (Teixell et al., 2005). Particularly, in the Middle Atlas and the Massif Central, Quaternary lavas were first emplaced along river valleys for tens of kilometres, and then incised by re-established rivers to form gorges. The uplift of Messinain (~7 Ma) shallow marine deposits in the Middle Atlas serves as a significant marker for constraining the lower limit of the timing of dynamic uplift (Babault et al., 2008). However, the upper limit of this timing is debated, and it is not clear if mantle-related uplift keeps sustaining the high topography of the Atlas system throughout the Quaternary (Lanari et al., 2022).

In this study, we took advantage of the distinctive geomorphic interaction between dated lava flows and main rivers in the Middle Atlas and the Moroccan Massif Central to calculate Quaternary fluvial incision rates. We combined the estimated post-eruption fluvial incision rates with topographic and fluvial DEM-based analysis and pre-existing data (e.g., ^{10}Be-dervied denudation rates, Clementucci et al., 2023b) to discuss the main factors that control fluvial incision and to investigate the tectonic and geomorphic evolution of this area of Morocco during the Quaternary.

2. Regional setting

The Atlas system is an intracontinental mountain belt that developed in the African plate of the Cenozoic Alpine belt (Fekkak et al., 2018; Gomez, 1996; Lanari et al., 2020). Geographically it spans from the Atlantic margin of Morocco to the Mediterranean coast of Tunisia for over 2000 km and forms a major morphologic barrier between the Sahara domain and the western Mediterranean Sea (Frizon De Lamotte et al., 2000). The High Atlas and the Middle Atlas represent the Moroccan part of this orogenic domain, which is bordered to the north by the alpine-type Rif belt and to the south, by the Paleozoic Anti-Atlas range (Fig. 1). The Mesetan domains (Western and Eastern Meseta) are made of Paleozoic terrains and their Mezo-Cenozoic cover (Hoepffner et al., 2005; Michard et al., 2023a) (Fig. 1 and 2). The Western Meseta consists

https://doi.org/10.5194/egusphere-2024-1746
Preprint. Discussion started: 20 August 2024

of several Paleozoic massifs deformed during the Variscan orogeny, separated by Meso-Cenozoic sedimentary series such as the Cretaceous-Cenozoic Phosphate plateau (Essaifi et al., 2014; Michard et al., 2023b; Ouanaimi et al., 2019). The Moroccan Massif Central, which is the largest massif of the Western Meseta, exhibits high elevation despite the lack of evidence of Cenozoic tectonic deformation (Barbero et al., 2011; Clementucci et al., 2023b; Yaaqoub and Essaifi, 2023).

The Middle Atlas is the NE trending branch of the Moroccan Atlas system. It runs obliquely from the WSW-ENE striking High Atlas near Beni Mellal in the Southwest until Taza in the Northeast where it is covered by the Neogene-Quaternary Taza-Guercif basin (Fig. 2). The post-Paleozoic geodynamic evolution of the Middle Atlas started with the Triassic and Jurassic rifting associated with the opening of the Atlantic and Tethys oceans (Beauchamp et al., 1996; Frizon De Lamotte et al., 2008; Jacobshagen, 1988). The extensional kinematic was controlled by zones of weakness inherited from the Variscan orogeny that affected the Meseta basement (Mattauer et al., 1977). Tectonic inversion in the Middle Atlas Mountains, driven by the convergence of the Africa and Eurasia plate, began in the late Cretaceous, with the main phase of uplift occurring during the Neogene (Charriere, 1984; Gomez et al., 2000; Lanari et al., 2023b).

Geomorphologically, the Middle Atlas can be divided, from the NW to the SE into two distinctive domains (Martin, 1981), the Tabular Middle Atlas (TMA) and the Folded Middle Atlas (FMA) (Fig. 1 & 2). The TMA is a weakly deformed area that consists mainly of Triassic and Liassic rocks. This sector exhibits a flat and high topography (mean elevation ~1500m) and sub-horizontal strata, which lie unconformably over the Palaeozoic basement of the Western Meseta, and it is traversed by a NE trending sinistral strike-slip fault, the Tizi-N-Tigheten fault. The FMA presents a high relief topography with four major narrow fault-related anticlinal ridges separated by three broad synclines (Colo, 1961; Gomez et al., 1998; Zafaty et al., 2023; Fig. 2). In addition to Triassic and Liassic sequences, thick and deep basin sequences related to tectonic subsidence were deposited in the FMA during the middle Jurassic (Charrière et al., 1994; Du Dresnay, 1988). Two major faults, namely the North Middle Atlas Fault (NMAF) that constitutes a limit with the TMA, and the South Middle Atlas Fault (SMAF), which separates the Middle Atlas from the peripheral foreland

https://doi.org/10.5194/egusphere-2024-1746
Preprint. Discussion started: 20 August 2024

(Missour basin), border the FMA. These faults are considered as the Middle Atlas paleo rift-bounding faults (Fedan, 1988). Accordingly, the FMA represents the paleo-rift basin whereas the TMA and Missour/High plateaux are its NW and SE margins respectively (e.g. Beauchamp et al., 1996).

The sedimentary record of the Middle Atlas is made of three megacycles separated by two sedimentary gaps (Boumir et al., 2023; Charrière, 1990; Frizon De Lamotte et al., 2008; Zafaty et al., 2023). The first megacycle (Trias-Malm) starts with Triassic continental deposits associated with tholeiitic basalts (Fig. 3), then the sedimentation becomes dominantly marine in the Lias-Malm with shallow-water carbonates accumulated in continental shelves and deep-water carbonates being deposited in subsiding basins (El Arabi et al., 2001). The second megacycle (Barremian-Eocene) corresponds mainly to littoral deposits with frequent evaporitic episodes in local depocenters along the western part of the Middle Atlas (Fig. 2). Finally, the last cycle (Tortonian to Plio-Quaternary) occurs mostly along the northern slope of the range and includes fluvio-alluvial continental deposits and shallow to moderately deep marine deposits (Fig. 2 and 3).

Restored geological cross-sections in the Middle Atlas yield a limited amount of Alpine crustal tectonic shortening of about 5km (Arboleya et al., 2004; Gomez et al., 1998). This moderate value is consistent with the low crustal root thickness of ~30 km estimated by geophysical studies (Ayarza et al., 2014; Makris et al., 1985; Tadili et al., 1986; Wigger et al., 1992). These aforementioned results, however, are in contrast with the high elevation of the Middle Atlas (mean elevation ~2000m), suggesting that the mountain chain is isostatically uncompensated at the crustal level (Gomez et al., 1998; Van Den Bosch, 1971), and that the crustal thickness cannot solely account for the high topography (Schwarz and Wigger, 1998). Lithospheric structure was then investigated in order to explain this discrepancy, and the results show a thin lithosphere beneath the Middle Atlas with a shallow, less than 80km, Lithosphere-Asthenosphere boundary (Fullea et al., 2010; Teixell et al., 2005; Zeyen et al., 2005). Accordingly, surface uplift of the Middle Atlas must be a combination of orogenic deformation and asthenospheric processes (Babault et al., 2008; Clementucci et al., 2023b; Missenard et al., 2006; Pastor et al., 2015; Teixell et al.,

https://doi.org/10.5194/egusphere-2024-1746
Preprint. Discussion started: 20 August 2024

2009). While the first component is well visible in the Cenozoic Middle and High Atlas belts, the second constitutes a long-wavelength, SW-NE oriented band that affects not only these belts but also the Anti-Atlas and the Meseta domains (Clementucci et al., 2023a; Missenard et al., 2006; Pastor et al., 2015). Babault et al., (2008) used scattered stratigraphic paleoelevation markers (e.g uplifted Messinian shallow-water marine sediments in the Skoura basin, northern Middle Atlas) to infer that the mantle-driven surface uplift occurred after the Messenian at a rate of ~0.2 mm/yr. Uplift, however, at least in the adjacent Western Meseta, may have already started in the late Cenozoic as suggested by stratigraphic data and river profile inversions that yielded uplift rates one order of magnitude lower (~0.05 mm/yr) than those recorded after the Messinian (Clementucci et al., 2023b).

The Middle Atlas was the site of significant volcanic activity during the Neogene-Quaternary (El Azzouzi et al., 1999, 2010; Berrahma, 1995; Harmand and Cantagrel, 1984; Rachdi, 1995). This volcanism is documented by mafic lava flows erupted from a hundred of well-preserved strombolian cones and maars, forming the Middle Atlas Volcanic Province (MAVP), the largest and youngest volcanic field in Morocco (El Azzouzi et al., 2010). The MAVP covers an area of ~ 960 km2 essentially within the TMA with scattered outcrops over the FMA (Fig. 2). El Azzouzi et al. (1999, 2010) carried out a petrologic-and geochemical study and a systematic K-Ar geochronological dating. This approach allowed to constrain the age (16.25Ma - 0.6Ma) of the lava flows, and to distinguish four lava types, namely Nephelinites, basanites, alkali basalts and subalkaline basalts. Nephelinites, which constitute 1.2% of the total surface of the MAVP, erupted only during two events: in the middle to late Miocene and in the Quaternary. The other three lava types are exclusively Plio-Quaternary in age (El Azzouzi et al., 2010; Harmand and Cantagrel, 1984). The MAVP is part of the intraplate, alkaline type, Cenozoic volcanism that affected Morocco (El Azzouzi et al., 2010) and is located within the elongated zone of thinned lithosphere described above (Missenard et al., 2006). The Neogene-Quaternary volcanism has contributed to reshape the landscapes of the Middle Atlas (Amine et al., 2019; Mountaj et al., 2019). Finally, the fluid lavas flowed through pre-existing valleys for dozens of kilometres before being incised by the current river streams (e.g., Bou Regreg, Oum Rbia and Sebou Rivers; Fig. 1).

https://doi.org/10.5194/egusphere-2024-1746
Preprint. Discussion started: 20 August 2024

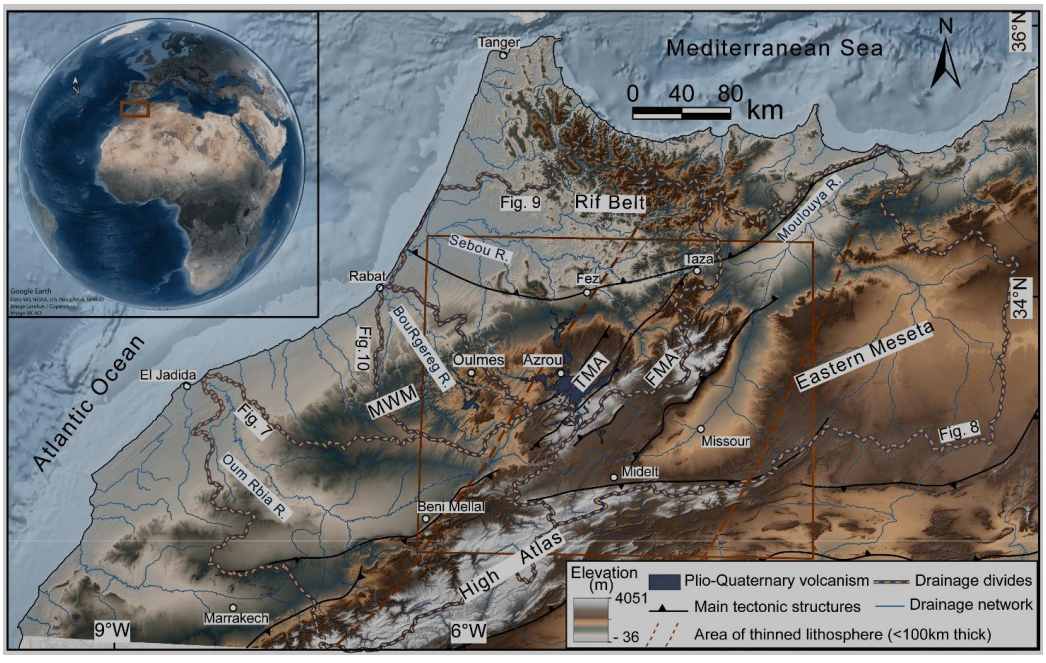

Figure 1: Digital Elevation Model (DEM SRTM 90m) of northern Morocco, with the main morphotectonic features. Inset map: Global view from Google Earth (2023). The area of thinned lithosphere is drawn after (Missenard and Cadoux, 2012). The location of figure 2 (Dark brown box), the watersheds of figures 5, 6, 7 and 8 (yellow dotted lines) are indicated. MWM: Moroccan Western Meseta, FMA: Folded Middle Atlas, TMA: Tabular Middle Atlas.

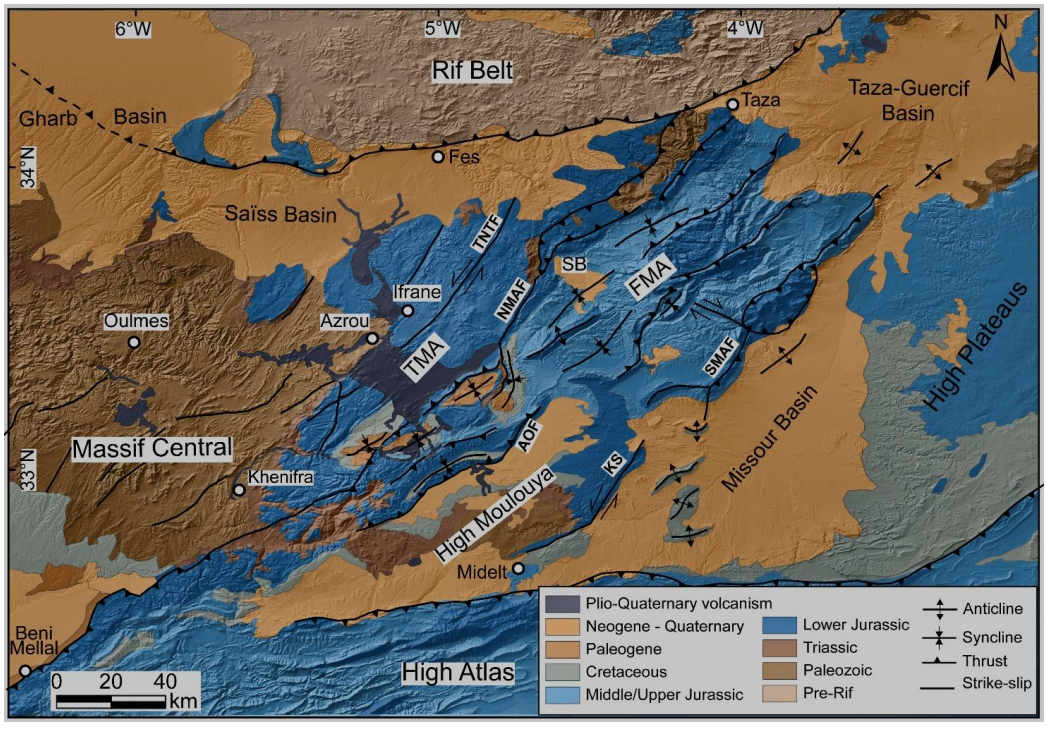

https://doi.org/10.5194/egusphere-2024-1746
Preprint. Discussion started: 20 August 2024

Figure 2: Simplified geological map of the Middle Atlas and surrounding areas (adopted from the geological map of Morocco (Hollard et al., 1985)). FMA: Folded Middle Atlas, TMA: Tabular Middle Atlas, SB: Skoura Basin, AOF: Ait Oufella Fault, KS: Ksabi Fault, NMAF: North Middle Atlas Fault, SMAF: South Middle Atlas Fault, TNTF: Tizi N'Tghetten Fault.

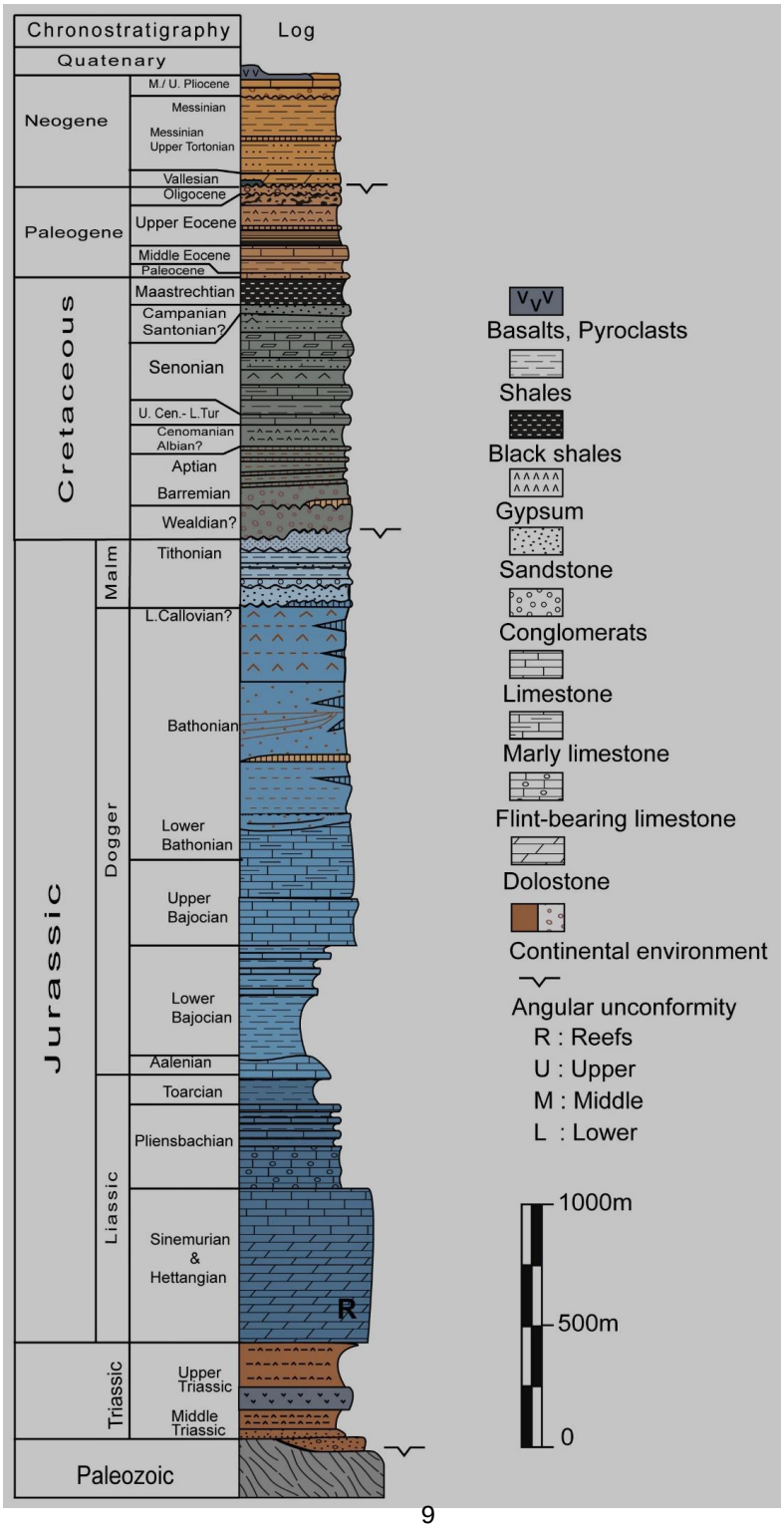

https://doi.org/10.5194/egusphere-2024-1746
Preprint. Discussion started: 20 August 2024

175

Figure 3: Synthetic stratigraphical column of the Middle Atlas (based on Boumir et al. (2023); Charrière (1990); Charrière and Haddoumi (2016); Fedan (1988)).

176 # 3. Methodology

177 ## 3.1. Topographic analysis

178 ### 3.1.1 Local relief and swath profiles

179

180 Topographic analysis provides first-order information about the degree of incision. To get such
181 information, we extracted topographic features (local relief maps and swath topographic profiles) from an
182 SRTM 90m DEM (Downloaded from https://srtm.csi.cgiar.org) using ArcGIS and MATLAB.

183 Local relief is a parameter describing the maximum dissection of a landscape owing to valley
184 incision (Kuhni and Pfiffner, 2001). It is defined by the subtraction between maximum and minimum
185 elevations within a sampling window. We generated the local relief map of the study area in ArcGIS by
186 means of range statistic in Focal statistics tool using a circular neighborhood of 1 km in radius.

187 Topographic swath analysis projects elevation values within a rectangular strip perpendicularly to
188 the midline of the strip. This elevation dataset is used to calculate statistical variables (typically, maximum,
189 minimum and mean) and to reveal specific characteristics of the topography that cannot be mapped with
190 one single profile (e.g., Telbisz et al., 2013). The curve of mean elevation gives the general topographic
191 signal of the landscape. The maximum elevations line marks ridgelines and, when associated with low slope
192 values, reveals paleo-surfaces. The minimum elevation profile corresponds to the valley floors. The
193 arithmetic difference between maximum and minimum elevations provides a quick estimation of the
194 topographic relief. Two swath topographic profiles were produced using the Topographic Analysis Kit (TAK)
195 (Forte and Whipple, 2019), which is built on the MATLAB-based scripts of Topotoolbox (Schwanghart and
196 Scherler, 2014). The width of the rectangles, fixed to 10 km, is large enough to enclose the elevation of

https://doi.org/10.5194/egusphere-2024-1746
Preprint. Discussion started: 20 August 2024

both major valleys and ridgelines. The profiles have been vertically exaggerated 10 times to enhance the topography given the long horizontal distance of the swaths.

3.1.2 Hypsometry

To characterize the stage of geomorphic development of the present-day catchments, we carried out a hypsometric analysis using the MATLAB functions developed by Jaiswara et al. (2020). The hypsometric analysis allows studying the distribution of the surface area with respect to the elevation in a drainage basin (Strahler, 1957). The hypsometric curve is constructed by plotting the relative height (h/H) against the relative area (a/A). A useful attribute of these curves is that drainage basins of different sizes can be compared, since area and elevation are plotted as functions of total area and total elevation (Keller and Pinter, 2002; Pérez-Peña et al., 2009). The hypsometric integral (HI) is defined as the area below the curve. This area represents the un-eroded volume of the basin. Varying between 0 and 1, the integral of a given catchment can be calculated as follows:

$$HI = \frac{mean\ elevation - minimum\ elevation}{maximun\ elevation - minimum\ elevation} \quad (1)$$

The shape of the hypsometric curve and the value of hypsometric integral for a given basin are related to its degree of dissection and hence to its evolution stage. Convex curves and high values of HI are indicative of a weakly eroded landscape (youthful stage); S-shaped curves and medium values of HI characterize moderately eroded regions (maturity stage) while concave curves and low values of HI are typical of a highly eroded topography (old stage) (Keller and Pinter, 2002; Schumm, 1956; Strahler, 1952).

3.2 River profiles and knickpoints analysis

River longitudinal profiles are plots displaying the variation in channel elevation versus its distance from the headwaters to the outlet. Modelling a river channel profile is critical to understand its incision history (Zhong et al., 2022). The stream power incision model (Howard and Kerby, 1983) is the most

https://doi.org/10.5194/egusphere-2024-1746
Preprint. Discussion started: 20 August 2024

commonly used model (Crosby and Whipple, 2006; Whipple and Tucker, 1999) for estimating relative changes in base-level and hence to quantify the minimum values of fluvial incision and to infer rock uplift patterns (Ballato et al., 2015; Boulton, 2020; Clementucci et al., 2023b; Lague, 2014)(Ballato et al., 2015; Boulton, 2020a; Clementucci et al., 2023b; Lague, 2014). The later model defines the variation over time of the river channel elevation (*dz/dt*) as the difference between the rock uplift (U) and the incision rate (I), with the incision rate being proportional to upstream drainage area, A, and river gradient, S:

$$\frac{dz}{dt} = U - I = U - KA^m S^n \quad (1)$$

Where *K* is a coefficient of erodibility and *m*, and *n* are positive constants.

Under steady state condition, the rock uplift rate and incision rate are in dynamic equilibrium, therefore the channel bed elevation does not change through time (*dz/dt* = 0). Accordingly, eq. (1) becomes:

$$S = \left(\frac{U}{K}\right)^{\frac{1}{n}} A^{-\left(\frac{m}{n}\right)} \quad (2)$$

Equation (2) describes a power-law relationship between channel gradient and drainage area, and is similar to the empirically Flint's equation (Flint, 1974):

$$S = ks\, A^{-(\theta)} \quad (3)$$

Where k_s= $(U/K)^{1/n}$ is the channel steepness that is sensitive to changes in rock uplift rate, rock types, climate, and θ = (m/n), which is the concavity index (Snyder et al., 2000; Whipple and Tucker, 1999). Deviations from this form indicate that the river is in transient state of disequilibrium as a result of base-level change (Siravo et al., 2021) and geomorphic features (knickpoints) may occur (Boulton, 2020).

From Flint's law (Eq. (3)), one can estimate the parameters *Ks* and θ by a linear regression of the bilogarithmic plot of S and A (Kirby and Whipple, 2012; Wobus et al., 2006). But given the covariance of *Ks* with θ, it is typical to normalize *Ks* (becoming k_{sn}) using a reference concavity (θ_{ref}), which is commonly set

https://doi.org/10.5194/egusphere-2024-1746
Preprint. Discussion started: 20 August 2024

to 0.45 (Kirby and Whipple, 2012). Moreover, this reference value has been calculated by minimising the scatter in χ space of all rivers draining the study area by Clementucci et al. (2023b).

We also used the integral approach (Perron and Royden, 2013; Willett et al., 2014), where the horizontal coordinate (x) of the river profile can be transformed into the χ-coordinate resulting in the transformed profiles or χ-plots. This method is an alternative to the slope-area analysis, which can be affected with noise embedded in DEMs.

By integrating Eq. (2) and considering U and K as constants in space and time, Eq. (4) can be obtained:

$$z(x) = z(x_b) + k_s A_0^{-\left(\frac{m}{n}\right)} \chi \quad (4)$$

$$\text{With} \quad \chi = \int_{xb}^{x} \left(\frac{A_0}{A(x)}\right)^{\frac{m}{n}} dx \quad (5)$$

Where x is the upstream distance from the outlet x_b, A is the drainage area and A_0 is a reference area.

We extracted the longitudinal river profiles, χ-plots, and the K_{sn} map using the ChiProfiler (Gallen and Wegmann, 2017). We only focused on river channels where incision rates from lava flows were estimated. The parameters were set as follows: θ_{ref} = 0.45, A_0 = 1 m^2 and A_{cri} = 10^6 m^2 (Critical drainage area, a threshold drainage area).

In order to classify the knickpoints, we checked them out using geological maps and Google Earth satellite images. Therefore, we labelled them as minor, lithological, and non-lithological. Minor knickpoints (blue circles) are those coincident with dams, and do not show significant variations in K_{sn} upstream and downstream or are just artifacts. Lithological knickpoints (yellow circles) are located between two lithologies with different rock strengths. Non-lithological knickpoints (Dark brown circles) are associated with important slope break in the profile and prominent low-gradient reach upstream.

3.3 Incision rates

https://doi.org/10.5194/egusphere-2024-1746
Preprint. Discussion started: 20 August 2024

The geomorphic relationship between river channels and Quaternary lavas flows in the Middle Atlas and the Moroccan Massif Central offers a good opportunity to quantify the fluvial incision rates. During their emplacement, the lava first flowed down the river channels (Fig. 4a) and then, once cooled, were incised by the same rivers. Following lava emplacement, if there is no substantial change in boundary conditions, such as a base-level drops and/or changes in precipitation regimes, the river would likely continue incising until it reaches its previous position marked by the lava-substrate stratigraphic limit (Fig. 4b). Otherwise, the fluvial incision would extend beyond that limit to adjust to any imposed perturbation (Fig. 4c). Dividing the current valley depth measured from the top of the lava flow by the age of the lava gives the rate of post-lava emplacement incision. In our study, valley depths were measured in the field using a GPS device (GARMIN GPS72H) and where suitable a meter stick, while lava flow ages were taken from available radiometric ages (El Azzouzi et al., 2010; Rachdi, 1995).

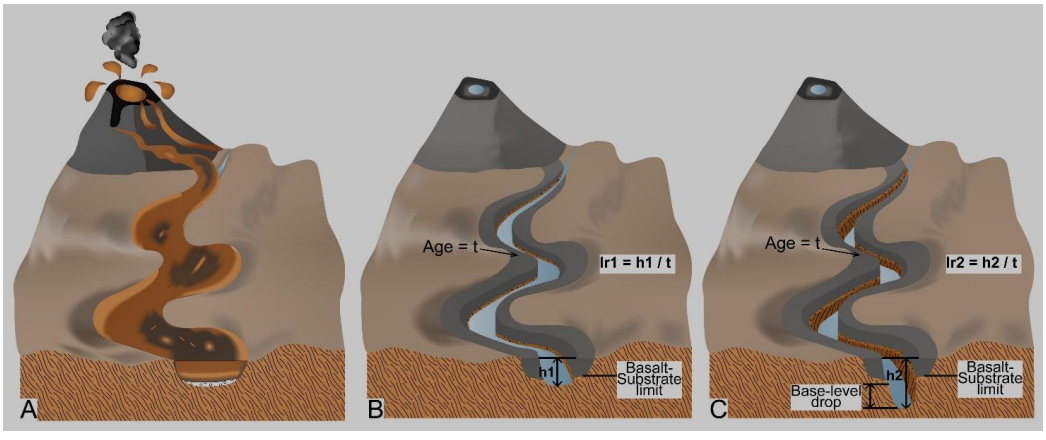

Figure 4: Schematic 3D diagrams depicting lava-rivers interactions. A) After the emplacement of a lava flow in a pre-existing river valley, the river will start incising the cooled lava until it attains its original base-level (B) it extends beyond the lava-substrate boundary in response to a prolonged base-level fall (C).

https://doi.org/10.5194/egusphere-2024-1746
Preprint. Discussion started: 20 August 2024

4. Results

4.1. Local relief and swath profiles

The local relief map (Fig. 5A) shows the highest values (480-1100m) in the Folded Middle Atlas (Between the NMAF and the SMAF), especially in its northeastern part near the major faults. The Tabular Middle Atlas exhibits mostly low values of local relief, that tend to slightly increase near the Tizi N'Teghtten and Dayet Aoua faults. The lowest values of local relief are found in the bordering Saïs sedimentary basin to the northwest, in the Taza-Guercif basin to the northeast and in the Missour basin to the southeast. The Massif Central shows an inhomogeneous distribution of local relief with values ranging from 270 to 580 m around Oulmes, that tend to decrease to the East along the corridor running between Azrou and Khenifra where they reach values of less than 270 m. While the lava flows exposed in the Bou Lahmayel valley (BLV) present relatively high local relief, ranging from 270 m to 580 m, the surface of the lava flows typically displays comparatively lower values, varying from 0 to 170 m. Nevertheless, the lava flows can be surrounded by zones of relatively high relief such as in the Guigou valley (GV) and southwest of Azrou where they range from 400 m to 580 m (Fig. 5A). The outlines of some river valleys are delineated by a noticeable contrast of local relief reflecting their high degree of dissection (e.g., Cheg El Ard Valley (CAV); Fig. 5A).

The topographic swath profiles (SW 1 and SW 2; Fig. 5B and C) are oriented WNW-ESE, perpendicular to the main structures of the Middle Atlas and surroundings and highlight the characteristics of the different morpho-structural domains of the study area. In the SW 1 swath, the Folded Middle Atlas shows high relief and consequently high fluvial incision (> 700 m). In contrast, the Tabular Middle Atlas (TMA), where most of the lava flows are located, represents an elevated low relief area with topographic relief not exceeding 300 m, while in the Saïss and Missour basins the maximum and minimum topography curves are very close indicating very low topographic relief. In the SW 2 swath, which runs from the Western Meseta to the High Moulouya and the Missour basin, the difference in the degree of incision

https://doi.org/10.5194/egusphere-2024-1746
Preprint. Discussion started: 20 August 2024

302 between the FMA and TMA is smoothed. The High Moulouya also exhibits a flat topography and a general
303 low incision except for the relief associated with the Ksabi fault. In contrast, the Central Massif shows high
304 relief and a topographic relief of about 500 m in the first 20 km of the profile and low topographic relief in
305 the second half of the profile.

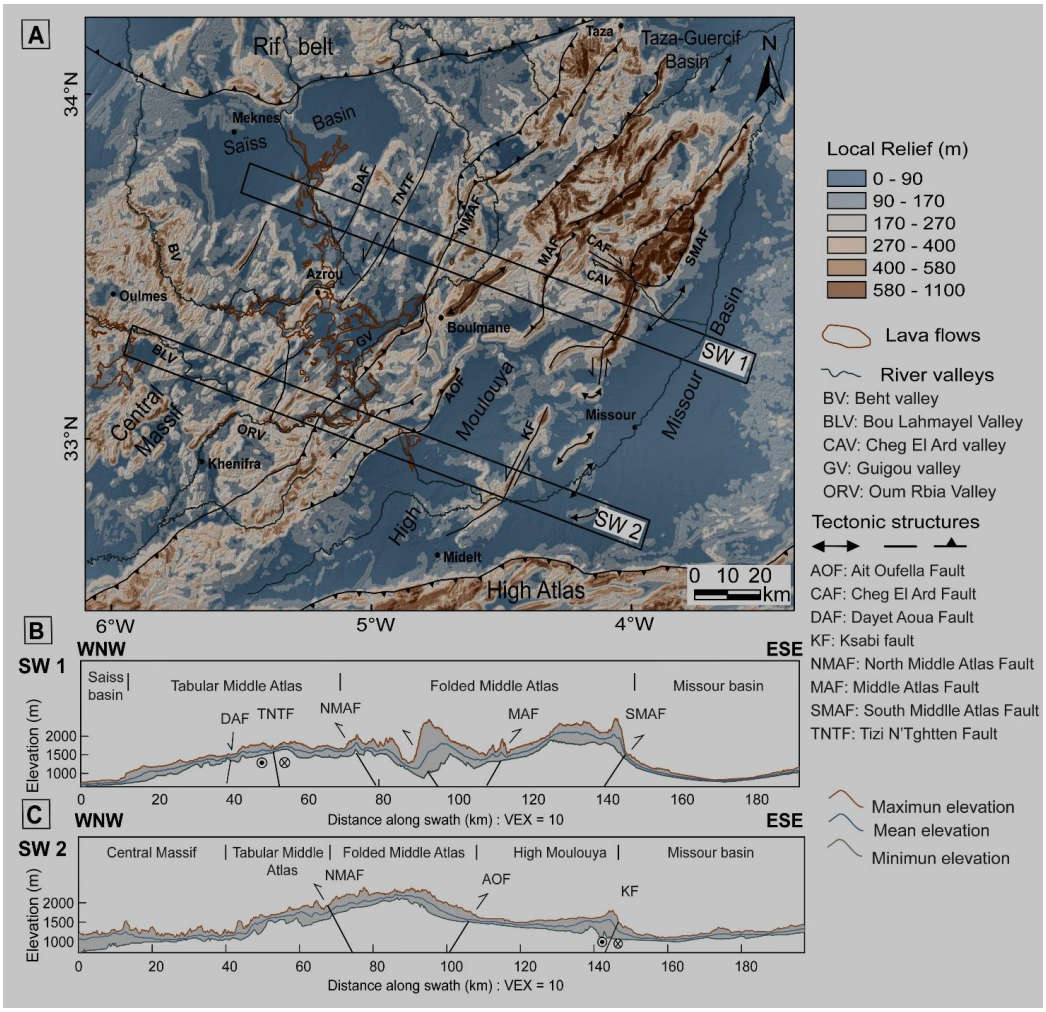

Figure 5: A) Local relief map of the Middle Atlas and surroundings with a 2 km moving window. B and C) Topographic swath profiles perpendicular to the main structures of the study area with their locations indicated in A.

306

307

https://doi.org/10.5194/egusphere-2024-1746
Preprint. Discussion started: 20 August 2024

4.2. Hypsometric and fluvial analysis

The drainage network in the Middle Atlas and surrounding plateaus includes four main rivers and related tributaries (Fig. 1). Three rivers, Oum Rbia, Bou Regreg and Sebou, are located on the western side of the belt and drain to the Atlantic Ocean. The Oum Rbia and Sebou rivers originate in the Middle Atlas while the Bouregreg originates in the Western Meseta. One river, Moulouya, is located on the eastern side of the belt and drains to the Alboran sea (western Mediterranean).

Notable variations in channel steepness are observed over the drainage network of the studied area (Fig. 6). The *Ksn* map shows generally higher values in the northeastern part of the Middle Atlas, especially in the river channels draining the NE fault-bounded front of the belt (SMAF). These high *Ksn* values are consistent with high local relief (Fig. 5A). The lowest values of *Ksn* are observed in the TMA, in the High Moulouya, and in the eastern part of the Massif Central. The river valleys where lava flows were

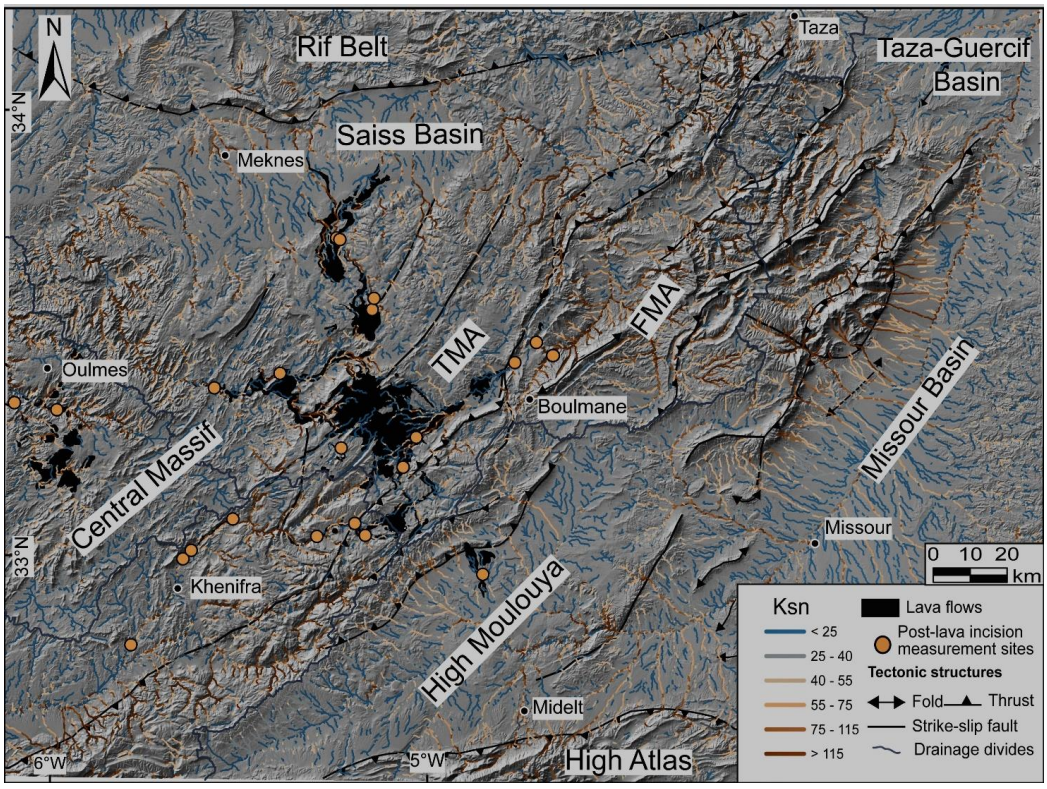

Figure 6: Normalized channel steepness indices (Ksn) of the Middle Atlas and surroundings, superimposed on a hillshade relief map.

https://doi.org/10.5194/egusphere-2024-1746
Preprint. Discussion started: 20 August 2024

emplaced generally exhibit low values of *Ksn*. However, it is noteworthy that the *Ksn* values are relatively higher in lava-bearing channels in the Massif Central south of Oulmès, than in the Middle Atlas.

4.2.1. Oum Rbia catchment

The catchment of Oued Oum Rbia has a W-E elongated shape with a drainage area of about 38000 km^2 and drains the southwestern termination of the Middle Atlas, the northwestern slopes of the High Atlas, and the southern slopes of the phosphate plateaus (Fig. 7A). The Oum Rbia River originates from the Oum Rbia springs which are located in the Middle Atlas domain. The trunk river has a length of 555 km from the springs to the outlet in the Atlantic Ocean. The main tributaries are those of its left bank namely Serrou, El Abid, and Tassaouat rivers. The trunk channel has a W-E trend in the Middle Altas, then it deviates to a NE-SW trend immediately at the exit of the Middle Atlas until the Tadla plain where the trend changes to a mean NW-SE direction.

The hypsometric curve of the Oum Rbia catchment is concave with a value of the hypsometric integral of 0.26 (Fig. 7C). Its longitudinal profile displays a series of knickpoints with different origins (Fig. 7D, E). The knickpoint located on the North Middle Atlas Fault is the most important one (Fig. 7B, D, E) since it depicts an abrupt change in the slope with a flat segment upstream (Fig. 5E). The lithological knickpoint (yellow circle) matches the transition between Eocene and Cretaceous strata. The Knickpoint (dark brown circle) just downstream of the lithological knickpoint is located upstream of the Oum Rbia sources and Mermel Fault (Fig. 7B). The knickpoints in blue correspond to dams.

https://doi.org/10.5194/egusphere-2024-1746
Preprint. Discussion started: 20 August 2024

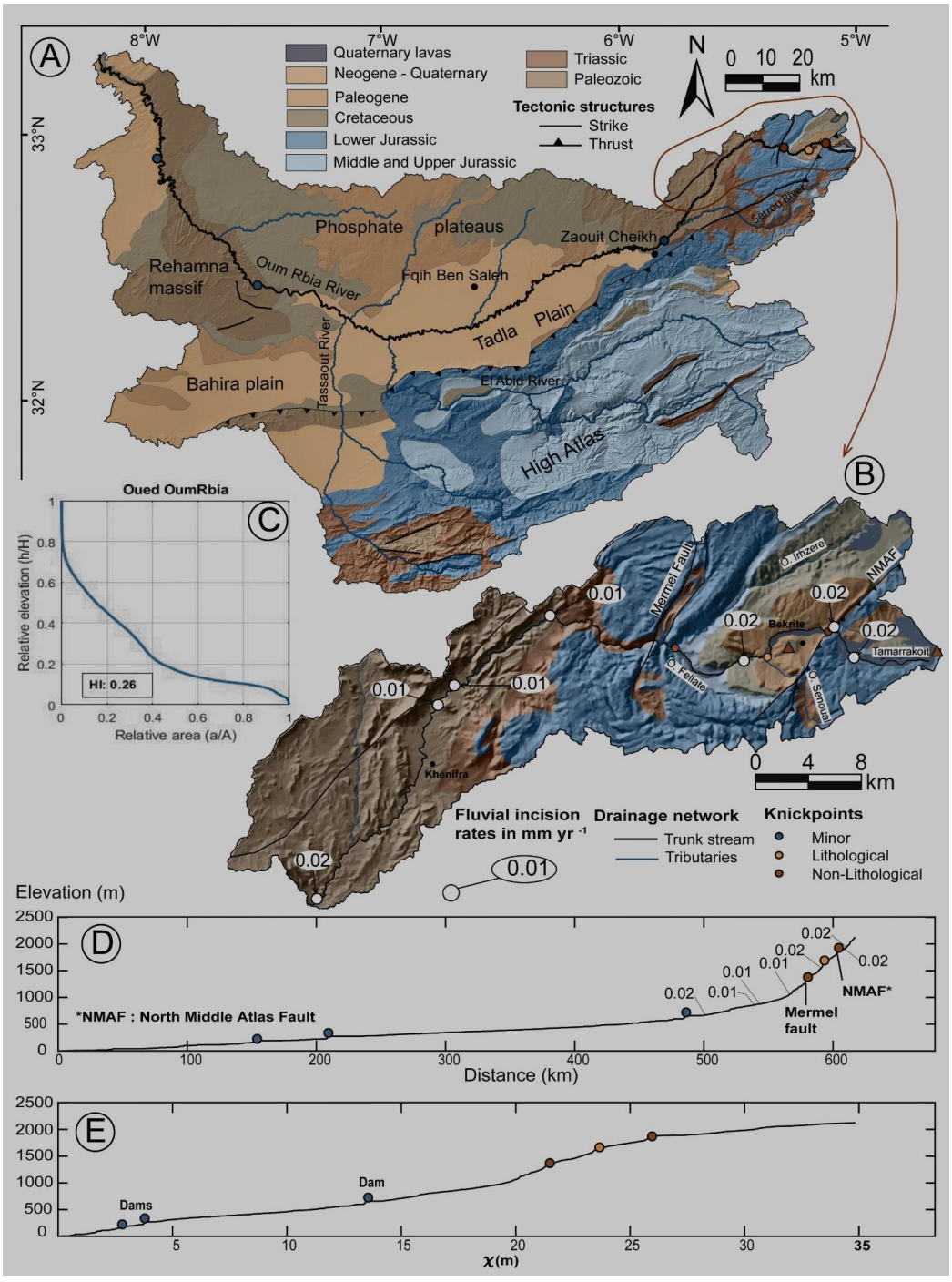

Figure 7: A) Simplified geological map of the Oum Rbia catchment, B) Close up view of upper course of the Oum Rbia with values of post-lava emplacement incision rates reported, C) Hypsometric curve and Integral index of the Oum Rbia catchment, and D) Longitudinal and E) Chi profile of the Oum Rbia River.

338

https://doi.org/10.5194/egusphere-2024-1746
Preprint. Discussion started: 20 August 2024

4.2.2. Moulouya catchment

The Moulouya drainage basin covers an area of about 60408 km^2 and drains the southeastern flank of the Middle Atlas, the northern flank of the High Atlas, the western slopes of the high plateaus, and the eastern Rif (Fig. 8A). The trunk channel is about 600 km long and trends SW-NE. Its sources are in the junction between the High and the Middle Atlas and its outlet is in the Mediterranean Sea.

The hypsometric analysis of the Moulouya catchment reveals an S-shaped hypsometric curve with a hypsometric integral value of 0.31 (Fig. 8B). Pastor et al. (2015) provided a detailed river profile and knickpoint analysis of the Moulouya River and its main tributaries. Here we focus only on the lava filled Tanfit River and, for comparison, the Cheg El Ard River where Pastor et al. (2015) calculated incision rates using fluvial terraces. The Tanfit channel shows a knickpoint (dark brown circle) located on the Paleozoic basement (Fig. 8A, C, and D) consistent with a local increase in the channel steepness (Fig. 6). The Moulouya River exhibits a minor knickpoint upstream of the Ksabi Fault (blue circle) and a non-lithological knickpoint in the Beni Snassen massif at the lower course of the river (Fig. 8A, C, and D). The Cheg El Ard River flows over the active southeastern deformational front of the Middle Atlas and coincides with the Cheg El Ard dextral fault CAV (Laville et al., 2007)). The Cheg El Ard longitudinal profile exhibits tree knickpoints (Fig. 8A, C, D). The uppermost knickpoint is prominent and well expressed in the Chi-plot (Fig. 8D) with a low-gradient reach upstream and a steep segment downstream. The knickpoint (blue circle) does not reveal a significant change in channel steepness upstream and downstream. The lowermost knickpoint coincides with the active Beni Aioun Anticline (BBA; Pastor et al., 2015).

https://doi.org/10.5194/egusphere-2024-1746
Preprint. Discussion started: 20 August 2024

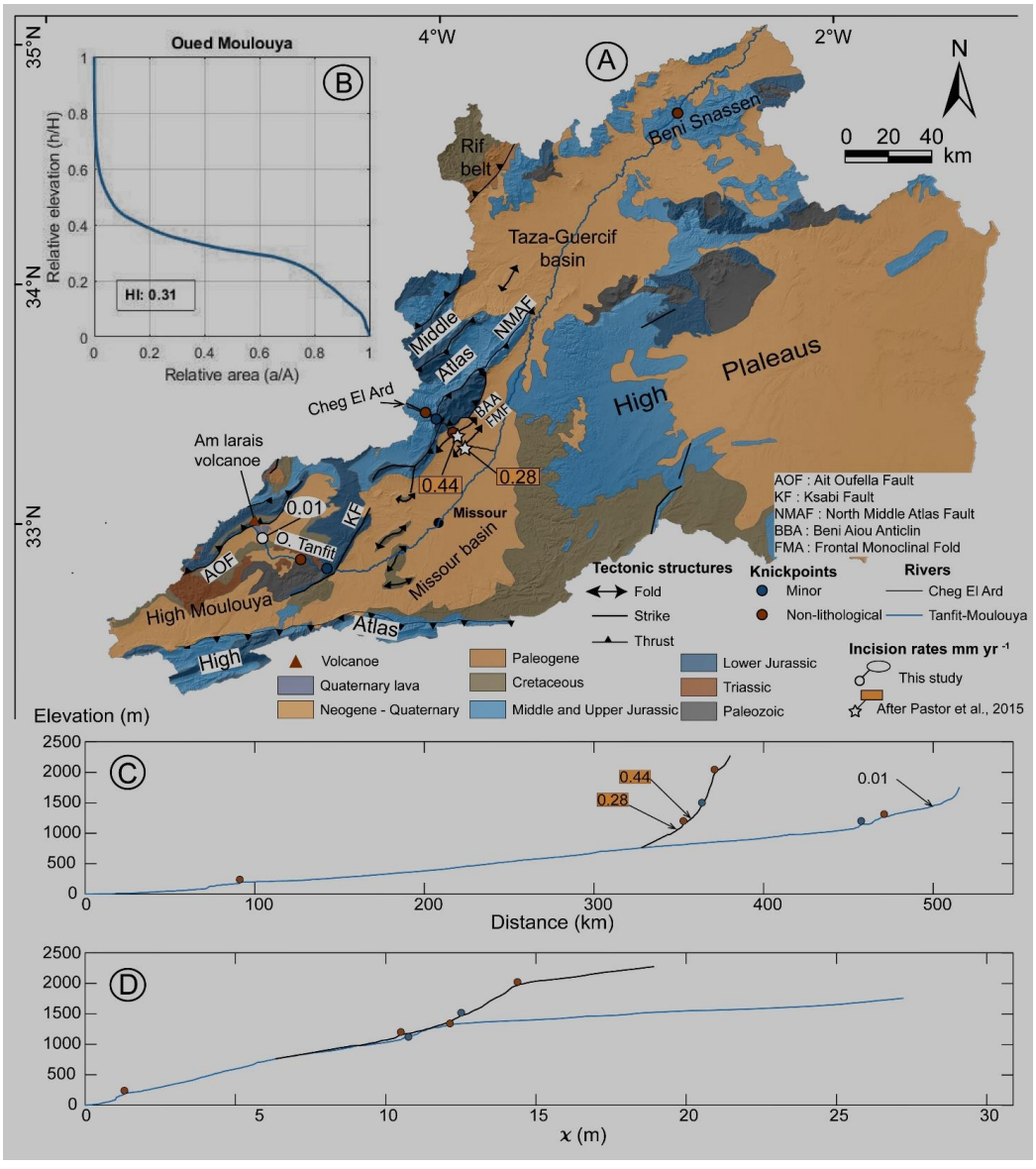

Figure 8: A) Simplified geological map, B) hypsometric curve and Integral index of the Moulouya catchment, C) Longitudinal and D) Chi profile of the Cheg El Ard and the Tanfit/Moulouya rivers.

358

https://doi.org/10.5194/egusphere-2024-1746
Preprint. Discussion started: 20 August 2024

4.2.3. Sebou catchment

The Sebou catchment has a roughly hexagonal shape and covers an area of 38718 km^2. The Sebou River drains the northern slopes of the Western Meseta, the northwestern slopes of the Middle Atlas, and the southern slopes of the Rif belt (Fig. 9A). The Sebou River originates from the Middle Atlas and flows into the Atlantic Ocean near Kenitra (Fig. 9A). The trunk channel is about 520 km long and flows towards the NW in the upper and middle course then it turns towards the West in the lower course. The Sebou River as well as its Middle Atlas tributaries flow through the Saïss Basin and cross over the Rifain frontal thrust before turning toward the Atlantic. The Sebou drainage basin shows a concave hypsometric curve and a hypsometric integral value of 0.22 (Fig. 9B). The concavity of the curve is related to the presence of the large Gharb basin in the lower part of Sebou catchment (Barcos et al., 2014).

The river longitudinal profiles of the three lava-filled channels present some knickpoints and knickzones that denote disequilibrium (Fig. 9C and D). The Sebou-Guigou river profile shows a 1200 m-high lithological knickpoint coinciding with the contact between the dolomitic and calcareous layers of the lower Jurassic and the marly limestone layers of the middle and upper Jurassic. A non-lithological knickpoint is identified in the Sebou River upstream the North Middle Atlas Fault (Fig. 9A, B, C). The longitudinal profile of Tizguite River exhibits a lithological knickpoint in the lower river course, at the end of lava flow, and a minor knickpoint in the upper reach. The river profile of Beht-Tigrigra displays a 500m-high knickpoint at about 250 km from the outlet (Fig. 9C). Downstream this knickpoint, the channel has entrenched deeply (Fig. 9A), and its steepness increases (Fig. 6). Clementucci et al. (2023b) provided data of denudation rates from ^{10}Be cosmogenic isotopes for the Beht-Tigrigra tributary showing values ranging between 19.5 to 40 m Ma^{-1} for the low-relief landscape (upstream of the knickpoint) and high-relief topography (downstream of the knickpoint), respectively.

https://doi.org/10.5194/egusphere-2024-1746
Preprint. Discussion started: 20 August 2024

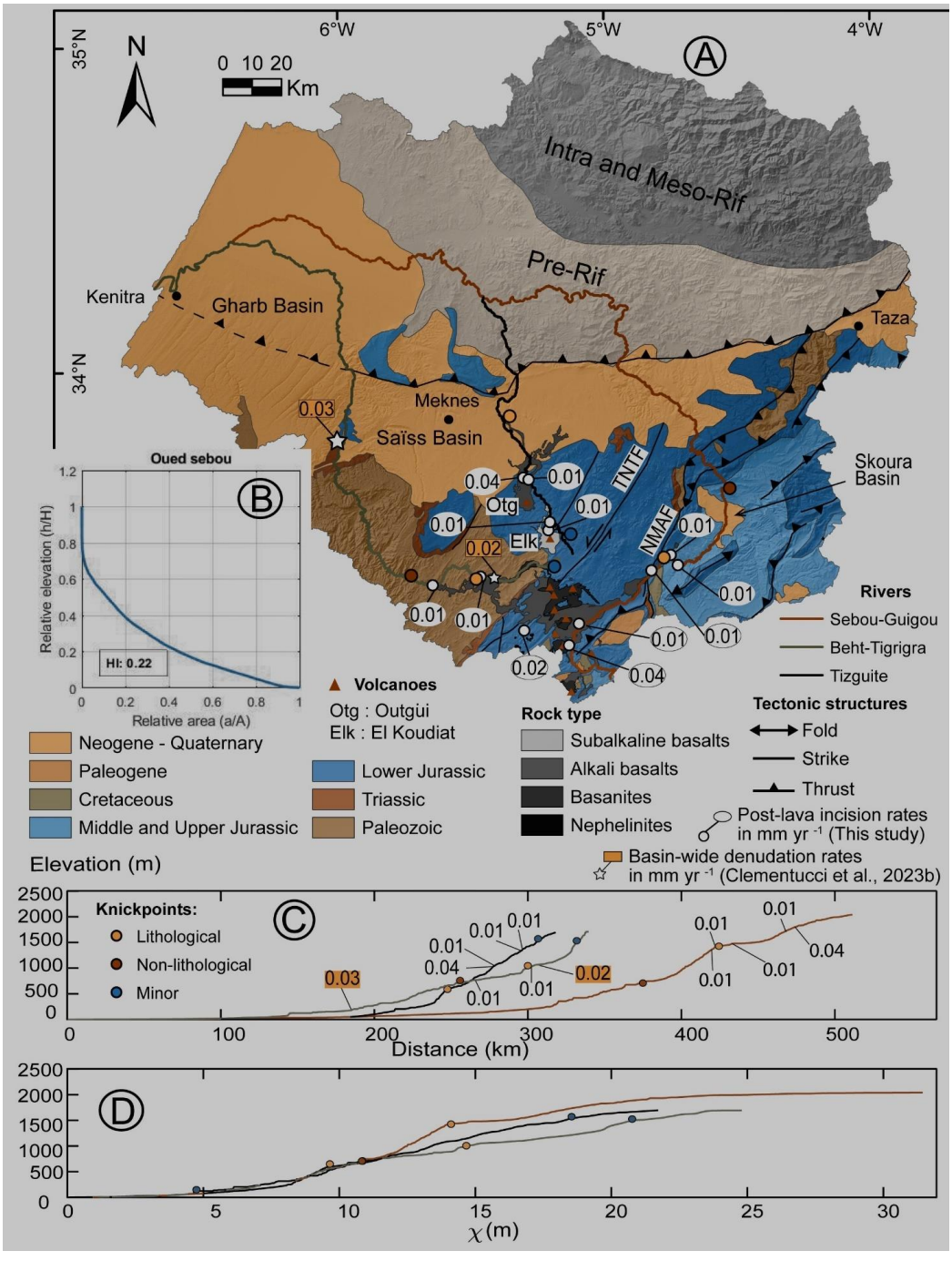

Figure 9: A) Simplified geological map, B) hypsometric curve and Integral index of the Sebou catchment, C) Longitudinal and D) Chi profile of the Sebou-Guigou, Beht-Tigrigra and Tizguite rivers.

381

https://doi.org/10.5194/egusphere-2024-1746
Preprint. Discussion started: 20 August 2024

4.2.4. Bou Regreg catchment

The Bou Regreg catchment is located within the western side of the Middle Atlas and has a fan-like shape with an area of 9834 km2. The river system drains the Paleozoic units of the Massif Central, which include from East to West: The Kasbat Tadla-Azrou anticlinorium, Fourhal-Tilt synclinorium, Khouribga-Oulmes anticlinorium, and the synclinorium of Romani in the lower course (Fig. 10A). The trunk channel has a mean NW-SE trend, and a length of ca. 250 km from its mouth in the Atlantic Ocean to its headwaters. Unlike the other rivers, the Bou Regreg does not reach the Middle Atlas. The hypsometric curve of the Bou Regreg catchment shows an S-shaped curve with a hypsometric integral value of 0.42, higher than those of the previously described watersheds (Fig. 10B).

The longitudinal profile of the lava-filled rivers (Bou Lahmayel-Bou Regreg and Ksiksou) are not concave-up profiles typical of an equilibrium state, but they show knickpoints highlighting the occurrence of some perturbations. The knickpoints, noted by the Dark brown circles, are 1000 m high and show prominent inflection in the profiles (Fig. 10C and D). The knickpoints assigned as minor do not present prominent slope break and in some cases, they may be artifacts. Here, basin-wide denudation rates range between 19.8 and 17.4 m Ma^{-1} for Bou Lahmayel-Bou Regreg and Ksiksou, respectively (Clementucci et al., 2023b).

https://doi.org/10.5194/egusphere-2024-1746
Preprint. Discussion started: 20 August 2024

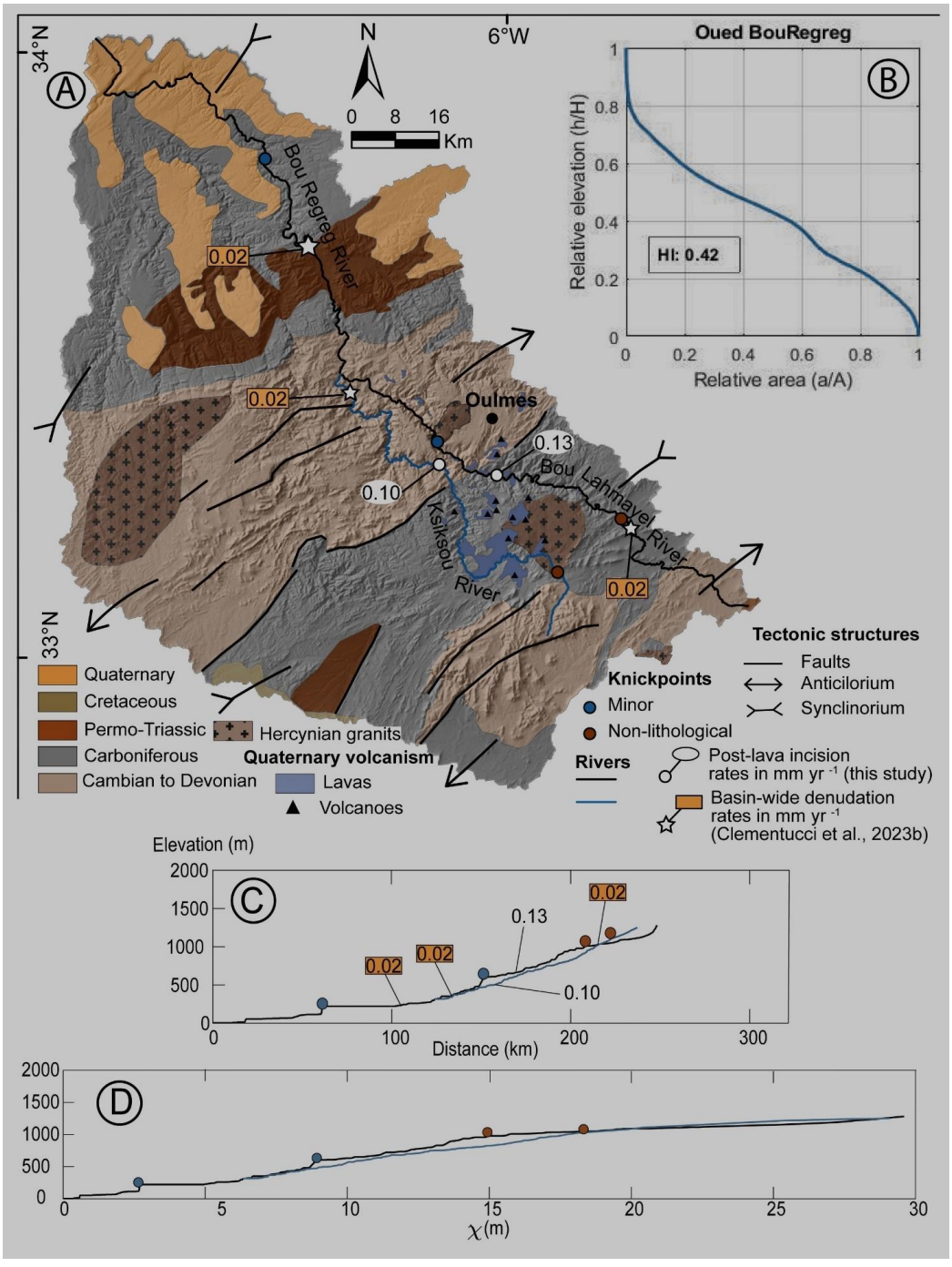

Figure 10: A) Simplified geological map, B) Hypsometric curve and Integral index of Bou Regreg catchment, C) Longitudinal and D) Chi profile of Bou Lahmayel and Ksikssou rivers.

398

https://doi.org/10.5194/egusphere-2024-1746
Preprint. Discussion started: 20 August 2024

4.3. Post-eruption incision

We estimated the post-lava emplacement incision rates in twenty-two sites distributed over the different morpho-structural domains of the studied area, namely, the Moroccan Massif Central, the Tabular Middle Atlas, and the Folded Middle Atlas. The measurements are scattered over the river valleys occupied by the lava flows (Fig. 11A; Table 1), which are distributed along the main rivers that drain the Middle Atlas and the surrounding plateaus.

https://doi.org/10.5194/egusphere-2024-1746
Preprint. Discussion started: 20 August 2024

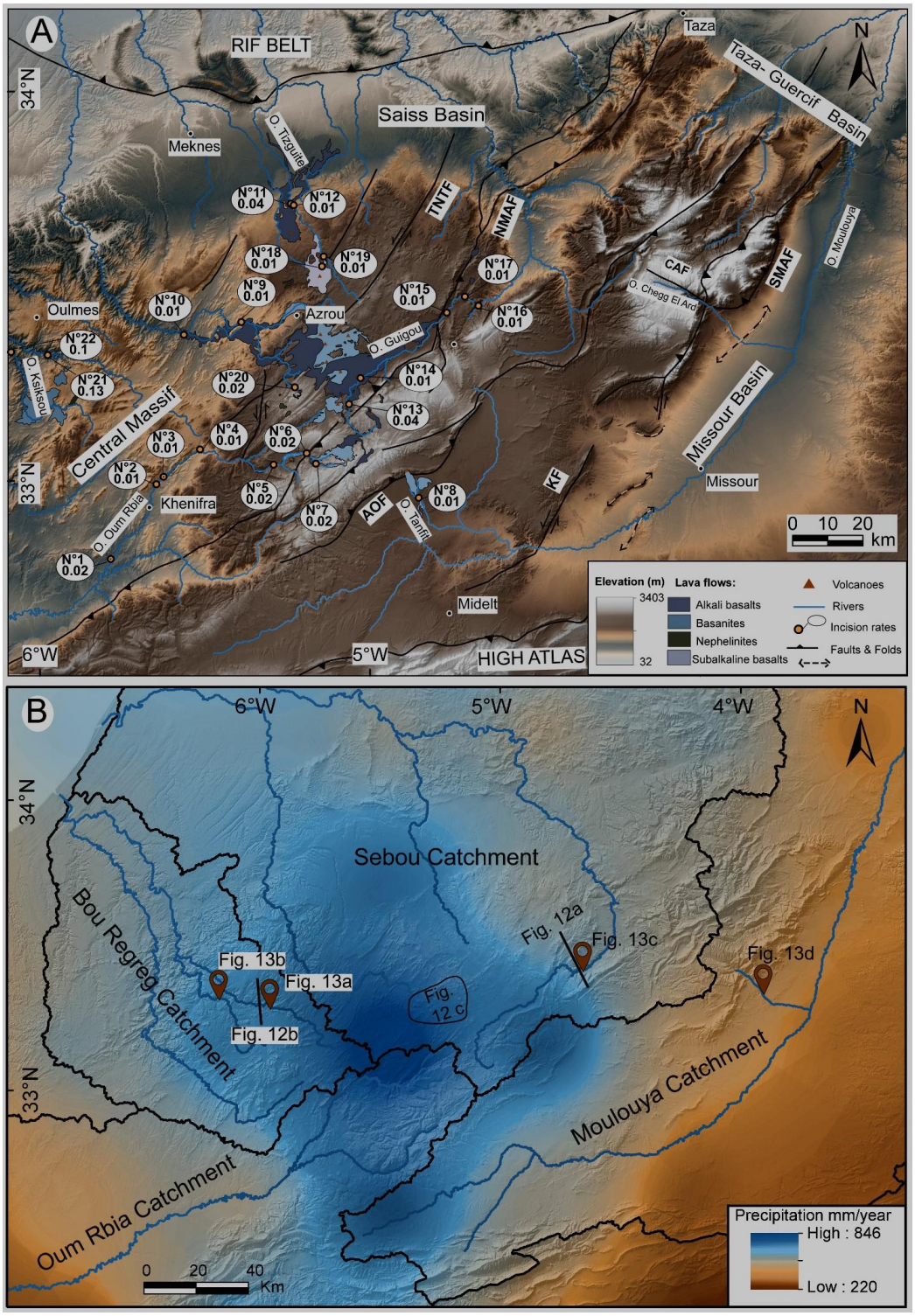

405 **Figure 11: A) Digital topography of the study area showing the post-lava incision rates, B) Average annual rainfall map from 1901 to 1981 using the data "CRU TS Version 4.06" from the Climatic Research Unit (University of East Anglia) and the National Centre for Atmospheric Science (NCAS) (https://crudata.uea.ac.uk/cru/data/hrg/). The locations of figures 12 and 13 are indicated.**

https://doi.org/10.5194/egusphere-2024-1746
Preprint. Discussion started: 20 August 2024

406 **Table 1: Summery of local post-lava fluvial incision rates in the Massif Central and the Middle Atlas. Lava ages are from El**
407 **Azzouzi et al., (2010).**

No.	Location	GPS Coordinates		Local post-lava incision (m)	Lava age (Ma)	Post-lava incision rates (mm/yr)	Rock type	Substratum rock type
		Longitude	Latitude					
1	Aourach bridge	-5.78915	32.80308	30	1.65 ± 0.08	0.02	Basanites	Schists
2	5km N of Khenifra	-5.6527	32.99626	13	1.65 ± 0.08	0.01		Not reached
3	El Borj	-5.63086	33.01562	20	1.65 ± 0.08	0.01		Not visible
4	Tanafnite	-5.52048	33.08681	14	1.65 ± 0.08	0.01		Not reached
5	Fellate	-5.29624	33.04903	36	1.65 ± 0.08	0.02		Limestones
6	Bekrit canyon	-5.19539	33.07887	30	1.65 ± 0.08	0.02		Limestones
7	Bou Anguar	-5.16721	33.05215	25	1.65 ± 0.08	0.02		Not reached
8	Am Larais	-4.85355	32.96532	22	1.56 ± 0.08	0.01		Limestones
9	Ait Youssef	-5.39753	33.415	23	2.19 ± 0.18	0.01	Alkali basalts	Not reached

https://doi.org/10.5194/egusphere-2024-1746
Preprint. Discussion started: 20 August 2024

10	Amghas	-5.57293	33.3812	32	2.19 ± 0.18	0.01		Schists
11	Outgui 1	-5.24838	33.71991	37	1.05 ± 0.26	0.04		Dolostones
12	Outgui 2	-5.23958	33.71626	13	0.89 ± 0.31	0.01		
13	Ait Qessou	-5.06698	33.20561	30	0.85 ± 0.07	0.04		Not reached
14	Ait Said Ouhaddou	-5.03209	33.27284	20	2.41 ± 0.28	0.01		Not reached
15	Charchara	-4.76885	33.44135	32	2.58 ± 0.12	0.01		Conglomerats
16	Taferdouste	-4.67204	33.45911	21	2.58 ± 0.12	0.01		Marls
17	Taghazoute	-4.71334	33.48271	19	2.58 ± 0.12	0.01		Limestones
18	Tizguit	-5.15165	33.55932	17	1.14 ± 0.11	0.01	Subalkaline basalts	Dolostones
19	Zaouia d'Ifrane	-5.14672	33.58471	9	1.14 ± 0.11	0.01		
20	Ain Kahla	-5.23267	33.24819	38	2.33 ± 0.1	0.02	Nephelinites	Not reached
21	Bou Tsaggatine	-5.99678	33.3289	122	0.93 ± 0.07	0.13	Tephrite	Metaturbidites
22	Bled	-6.107813	33.34059	110	1.1 ±	0.10	Basanites	

https://doi.org/10.5194/egusphere-2024-1746
Preprint. Discussion started: 20 August 2024

	Belmadi				0.1			

408

409 4.3.1. Moulouya catchment

410 The lava flows used in this study within the Moulouya watershed erupted from the Am Larais
411 volcano (Fig. 8A). The lavas flowed for about 14 km along the Tanfit River, a tributary of the Moulouya
412 River. These volcanic rocks are basanites and have a K/Ar radiometric age of 1.56 ± 0.08 Ma (El Azzouzi et
413 al., 2010) . Our field observations show that these Quaternary lavas cross the Ait Oufella fault (Fig. 6A). The
414 post-lava emplacement incision depth, undertaken upstream of the non-lithological knickpoint in the Tanfit
415 River (Fig. 8A and D), is about 22 m, which corresponds to an incision rate of 0.01 mm yr^{-1}.

416 4.3.2. Oum Rbia catchment

417 The lava flows in the Oum Rbia River erupted from the Tamarrakoït volcano (Martin, 1981). These
418 lavas are also basanites and were dated in two localities (El Azzouzi et al., 1999; 2010). In El Borj (5 km
419 North of Khenifra) they yielded a K/Ar age of 1.01 ± 0.04 Ma and near the Bekrite village they yielded a K/Ar
420 age of 1.65 ± 0.08 Ma (Fig. 7B). The lavas flowed for about 90 Km from the Middle Atlas to the Western
421 Meseta along the Oum Rbia River and its upper tributaries (Fellate and Amengous Rivers; Fig. 7B). Our field
422 observations, indicate that these Quaternary basanites cross the NMAF. The incision rate into the
423 Quaternary lava was measured in seven stations along the river upstream and downstream of knickpoints.
424 The magnitude of fluvial incision of the lavas varies from 13 to 36 m indicating incision rates between 0.01
425 and 0.02 mm yr^{-1}.

426 4.3.3. Sebou catchment

427 The majority of the lava flows of the studied area is circumscribed within the Sebou watershed (Fig.
428 9A). They erupted from the volcanic centres distributed over the tabular Middle Atlas and flowed along pre-
429 existing valleys to the plains of the hinterland (Martin, 1981). The lavas flowed mainly along the Guigou,
430 Tizguit and Tigrigra tributaries. Along the Guigou channel, alkali basalt lava flows that travelled for about 40
431 km to eventually stop in the Skoura Basin, yielded K/Ar ages of 2.41 ± 0.28 and 2.58 ± 0.12 Ma (El Azzouzi

https://doi.org/10.5194/egusphere-2024-1746
Preprint. Discussion started: 20 August 2024

et al., 2010). Along the Tizguite channel, alkaline and subalkaline lavas were emitted from two main volcanoes (Elkoudiat and Outgui) and flowed for a cumulative length of about 35 km. The lavas erupted from the Outgui Volcano are alkali basalts with a mean K/Ar age of 1.61 Ma, while the lavas from the El Koudiat volcano are subalkaline basalts and have a mean K/Ar age of 1.05 Ma (El Azzouzi et al., 2010). The lavas also flowed from the Tabular Middle Atlas towards the lowland of the Massif Central along the Tigrigra valley and other steep ravines for about 50 km. The volcanics used to measure incision rates in the Tigrigra valley, are alkali basalts and yielded a K/Ar age of 2.19 ± 0.12 Ma (MA412 sample of El Azzouzi et al., 2010). Our field observations indicate that lavas in the Tabular Middle Atlas cross the Tizi N'Tghetten strike-slip Fault without being deformed by the fault (TNTF; Fig. 9A). The vertical incision into the lavas varies from 9 to 38 m which, together with the K/Ar ages, indicate post lava incision rates between 0.01 and 0.04 mm yr^{-1}.

4.3.4. Bou Regreg catchment

The lava flows encompassed in the Bou Regreg catchment erupted from about twenty volcanoes. The lavas flowed for about twenty kilometers along the Bou Lahmayel and Ksiksou Rivers, which are tributaries of the Bou Regreg River (Fig. 10). The lava flows, we have used for the incision rate calculation, are tephrites in the Bou Lahmayel River and basanites in the Ksikssou River (Baudin et al., 2001; Bouhdadi et al., 2002). Their K/Ar ages are 0.93 ± 0.07 and 1.10 ± 0.10 Ma respectively (Rachdi, 1995). The vertical incisions into the lava flows are 122 m in the Bou Lahmayel River and 110 m in the Ksiksou River. Combined with the K/Ar ages, they indicate incision rates of 0.13 and 0.10 mm yr^{-1} respectively. Both measurements are located downstream of the non-lithological knickpoints (Fig. 10A and C). It noteworthy that the post-lava emplacement fluvial incision measured in the Bou Regreg catchment goes several tens of meters beyond the lava-substrate interface (Fig. 12B and 13A).

To summarize, the magnitude of post-lava emplacement incision varies between 9 and 38 m in twenty measurement sites (Sites N°1 to N°20), while it reaches 110 m and 122 m in two sites located in the Bou Regreg catchment (Table 1; N°21 and 22). The lava flows are Quaternary with radiometric ages varying

https://doi.org/10.5194/egusphere-2024-1746
Preprint. Discussion started: 20 August 2024

between 2.58 and 0.85 Ma. The calculated incision rates range between 0.01 and 0.13 mm yr^{-1}. The incision rates are not correlated with the ages of the lava flows. The incision rates calculated in the Bou Regreg catchment (0.1-0.13 mm yr^{-1}) are one order of magnitude higher than those calculated in the other river catchments, as also shown by available basin-wide erosion rates for the same region averaged over a time scale of few tens of thousands of years (Clementucci et al., 2023b).

5. Discussion

The 2.58- to 0.85 Ma-aged lavas exposed along the valleys of the Middle Atlas and the Massif Central allow us to calculate post-lava emplacement fluvial incision rates. Combined with topographic and fluvial analysis, this dataset help constraining the evolution of the landscape at regional scale (Middle Atlas and surroundings) over the Quaternary. Overall, we observe one order of magnitude difference in incision rates between the Western Meseta and Middle Atlas. The Massif Central shows relatively high post-Quaternary incision rates in the order of 0.1 mm yr^{-1}, while the other locations present rather uniform incision rates of about 0.02 mm yr^{-1}. Our geomorphic analysis is consistent with this dichotomy in fluvial incision rates between the Bou Regreg catchment and the other catchments. As such, higher local relief and hypsometric index values are relatively higher in the Massif Central sector with respect to the Middle Atlas domain.

Many studies have interpreted incision rates in terms of rock uplift (Clementucci et al., 2023b; Evenstar et al., 2020; Lavé and Avouac, 2001; Ott et al., 2018; Pan et al., 2013; Pastor et al., 2015; Wu et al., 2020), however, there are other factors, such as climate and lithology that can influence the rate of incision (Campforts et al., 2020; Clementucci et al., 2022). Below we discuss the effect that each of these three mechanisms may have had on the observed spatial variations of incision rates between the Western Meseta and the Middle Atlas.

5.1. Lithology

https://doi.org/10.5194/egusphere-2024-1746
Preprint. Discussion started: 20 August 2024

Bedrock is known to exert a significant impact on the rate of erosion (Clementucci et al., 2022; Montgomery and Gran, 2001; Moumeni et al., 2024; Sklar and Dietrich, 2001; Zondervan et al., 2020). Due to differences in mineral composition and chemical structure, different rock types have varying levels of resistance to erosion (Burbank and Anderson, 2011), and less-resistant lithologies tend to be incised more easily than high-resistant lithologies (e.g. Clementucci et al., 2022; Zondervan et al., 2020). Rock-strength data from the adjacent High Atlas indicate that Paleozoic meta-sediments and Mesozoic limestones have similar Uniaxial Compressive Strength UCS, with average values of 55 and 57 MPa, respectively (Zondervan et al., 2020). Both lithologies are widely exposed in the Massif Central and Middle Atlas and hence constitute the substrates for lava flows. Nevertheless, our estimated incision rates show one order of magnitude difference between the Middle Atlas and the Western Meseta (table 1). This observation suggests that lithology cannot fully account for the observed spatial variations in incision rates, at least on a Quaternary time scale.

5.2. Climate/Precipitation

Climate is another major factor that controls surface processes and thus erosion rates (England and Molnar, 1990; Ferrier et al., 2013; Hartshorn et al., 2002; Willett et al., 2001). An increase in precipitation, and thus in rivers runoff, enhances the capacity of rivers to incise (Lin et al., 2021; Pérez-Peña et al., 2009; Whipple, 2009). Analogue and numerical modelling also suggest that a gradient in precipitation can lead to differential erosion rates and then to divide migration towards the drier side of an orogen (Bonnet, 2009; Reitano et al., 2023; Willett, 1999). To investigate the potential impact of climate on erosion rates, many studies used modern precipitation rates as proxy for climatic forcing (e..g., Champagnac et al., 2012; Palumbo et al., 2010; Pan et al., 2010; Struth et al., 2020; Winiger et al., 2005; Wu et al., 2020). Figure 11B shows the average annual precipitation map of the study area during the period 1981-2011 interpolated using data from the Climatic Research Unit (University of East Anglia) and the Met Office (Harris et al., 2020). The rainfall map does not reveal any significant contrast in precipitation between the Bou Regreg

https://doi.org/10.5194/egusphere-2024-1746
Preprint. Discussion started: 20 August 2024

catchment, in which we measured higher incision rates, and its surrounding watersheds. The highest precipitation, around 800 mm yr^{-1}, falls in the triple junction of the Bou Regreg, Oum Rbia, and Sebou drainage divides. In addition, most of the Moulouya catchment receives lower precipitation in comparison with the other catchments, although data from Pastor et al., (2015) showed high fluvial incision rates in the Cheg El Ard valley (Fig. 8). Therefore, based on the precipitation pattern represented in figure 11B and assuming that this distribution remained similar during the Quaternary, the rainfall spatial gradient alone cannot explain the spatial variation of our fluvial incision rates. The apparent independence of basin-wide denudation rates on precipitation is also testified in the recent work conducted by Clementucci et al. (2023b) in the same study area using IMERG data.

5.3. Surface uplift

Given that lithology and climate fail to account for the spatial variation in fluvial incision rates, we explore rock uplift induced by tectonic, and mantle-driven processes as potential cause. The Moroccan Massif Central constitutes the largest massif of the Paleozoic Western Meseta realm. These terrains consist of metamorphic and magmatic rocks that were assembled during the Variscan orogeny (Michard et al., 2023). Previous studies characterized this region as tectonically stable following the Hercynian orogeny (e.g, Michard, 1976). However, recent studies have provided new insights, revealing that this area has undergone vertical movement during the Mezo-Cenozoic times (Barbero et al., 2011; Clementucci et al., 2023b; Ghorbal et al., 2008; Yaaqoub and Essaifi, 2023). On the other hand, the Middle Atlas is a Cenozoic intracontinental belt that resulted from the tectonic inversion of a Triassic-Jurassic rift that once affected the Moroccan Meseta (Charrière, 1990). The tectonic inversion of the Middle Atlas began in the late Cretaceous and culminated during the Oligocene-Neogene (Charrière, 1990). The uplift of the Middle Atlas is the result of the superposition of mantle-driven uplift and tectonic uplift related to the Cenozoic shortening (Babault et al., 2008; Clementucci et al., 2023b; Lanari et al., 2023; Pastor et al., 2015).

https://doi.org/10.5194/egusphere-2024-1746
Preprint. Discussion started: 20 August 2024

The inferred Quaternary incision rates from the lava flows in the Middle Atlas are one order of magnitude lower than the estimates for the Moroccan Central Massif. The analysis of geomorphic indices such as local relief (Fig. 5) and channel steepness (k_{sn}; Fig. 6), which is a proxy for rock uplift assuming similar rock erodibility and precipitation rates and also in case of equilibrated river profiles (e.g., Ahnert, 1970; Kirby and Whipple, 2012; Safran et al., 2005; Wu et al., 2020), mimics the distribution of the incision rates with lower values that are typically observed in the Middle Atlas. Moreover, the hypsometric analysis of the Bou Regreg river reveals a high hypsometric index (Fig. 10B) suggesting that the Bou Regreg catchment is still in a young stage of geomorphic evolution (e.g, Barbero et al., 2011). This geomorphic immaturity is also illustrated by the river longitudinal profiles of the lava-filled valleys (Fig. 10 C and D), which exhibit elevated non-lithological knickpoints indicating topographic transience most likely triggered by changes in surface uplift rates (e.g., Clementucci et al., 2023b).

Our Quaternary incision rates in the Bou Regreg watershed, draining the Moroccan Massif Central, are in the order of 0.1 mm yr^{-1}. These rates are comparable in magnitude to those presented by Pastor et al. (2015) for the last 411 ka and the uplift rates, averaged over the last 5 Ma, estimated by Babault et al. (2008). Pastor et al. (2015) combined fluvial geomorphic analysis and incision rates from Quaternary river terraces in the Cheg El Ard valley to infer the recent tectono-geomorphic evolution of the Missour basin and the surrounding Middle Atlas and High Plateaus hinterlands. The occurrence of incised and undeformed fluvial terraces in the tectonically quiescent distal part of the Missour Basin was interpreted to reflect a regional dynamic topography with uplift rates of 0.1-0.2 mm yr^{-1} (Babault et al., 2008, Pastor et al., 2015). Conversely, the fluvial incision rates value of 0.44 mm yr^{-1}, calculated near the Middle Atlas front (Fig. 8), in an area affected by recent fault-propagation folds, indicate incision related to the combined effect of regional dynamic uplift (≈0.1-0.2 mm yr^{-1}) and local thrust-related uplift (≈0.3 mm yr^{-1}). Thus, the main conclusion of these studies was that the regional surface uplift results from the combination of mantle-driven surface uplift and structural surface uplift produced by the frontal structures of the Middle Atlas. Given that there is no evidence indicating that the Moroccan Massif Central was affected by Neogene

https://doi.org/10.5194/egusphere-2024-1746
Preprint. Discussion started: 20 August 2024

558 tectonic shortening (Barbero et al., 2011), the post-lava emplacement incision rates we measured must be
559 related to mantle-related surface uplift.

560 On the other hand, the fluvial incision rates measured from the lava flows in the watersheds that drain
561 the Middle Atlas Mountain belt (Fig. 7, 8, 9) are in the order of 0.01 mm yr^{-1}. These values are significantly
562 lower than those related to the tectonic uplift reported in the eastern flank of Middle Atlas by Pastor et al.
563 (2015). It is worth noting that the eastern flank of the Middle Atlas where the thrust-related (≈0.3 mm yr^{-1})
564 incision rates were calculated, is bounded by the SMAF, which is an active complex fault zone, where
565 Jurassic carbonates are thrusted onto coarse-grained deposits of the Neogene-Quaternary Missour basin
566 (Delcaillau et al., 2007; Laville et al., 2007). Therefore, the Cheg El Ard River, which drains the tectonically
567 active Jbel Bou Nacer (the highest summit in the Middle Atlas) and crosses the active fault-related folds
568 associated with the SMAF, is such a powerful river that has entrenched deep and narrow canyons (Fig.
569 13D). In contrast, the western flank of Middle Atlas, where we calculated the majority of incision rates,
570 lacks evidence of Quaternary tectonic uplift. Rather, the reported recent tectonic activity is accommodated
571 by strike-slip movements with no significant relief building (e.g., Ait Brahim et al., 2002; El Azzab and El
572 Wartiti, 1998; Fedan and Thomas, 1986; Hinaje et al., 2019). As a matter of fact, unlike the eastern flank of
573 the Middle Atlas, the western one is devoid of a well-developed synorogenic flexural foreland basin,
574 suggesting that tectonic shortening is primarily accommodated by thrusting along the SMAF. This could be
575 explained by late Neogene partitioning of oblique deformation, such that strike-slip kinematics was
576 accommodated along the NMAF, while thrusting occurred along the SMAF (Gomez et al., 1998).
577 Furthermore, our field observations suggest that the Quaternary lava flows cover the major faults in
578 western side of the Middle Atlas, i.e. Tizi N'Tghatten Fault (Fig. 9A) and the North Middle Atlas Fault (Fig.
579 7B). This indicates that the low post-lava emplacement incision rates calculated on the western flank of the
580 Middle Atlas could reflect the lack of substantial Quaternary thrust-related surface uplift.

581 Additionally, the Quaternary incision rates in the Middle Atlas are also lower than those attributed to
582 the mantle dynamic uplift estimated by Pastor et al. (2015). Interestingly, despite the large wavelength of
583 this component of surface uplift (Clementucci et al., 2023b; Frizon de Lamotte et al., 2009; Lanari et al.,

https://doi.org/10.5194/egusphere-2024-1746
Preprint. Discussion started: 20 August 2024

2023; Missenard et al., 2006; Pastor et al., 2015), the Quaternary incision rates in the Middle Atlas do not appear to record such an uplift. This disparity could be explained as a fluvial response to the mantle-related uplift documented in the Massif Central (Clementucci et al., 2023b). It appears that this perturbation (e.g., erosional wave) has not yet reached the localities where we measured post-lava emplacement incision rates, resulting in the topography remaining in a transient state. This is consistent with the fact that most of our lower incision rates were calculated upstream of the non-lithological knickpoints (Figs. 7, 8, 9 and 10). In contrast, the incision rates calculated in the Oum Rbia River represent an exception as they are of the same order of magnitude as elsewhere in the Middle Atlas although being measured downstream of the river major knickpoint (Fig. 7). This knickpoint may not be linked to mantle-related uplift but to a base-level fall due to drainage reorganization of the Oum Rbia River during the late Pliocene (Yaaqoub and Essaifi 2023).

Another possibility for explaining the slower post-lava emplacement incision rates in the Middle Atlas with respect to the Moroccan Massif Central could be that localized surface uplift is affecting exclusively the Massif Central. Clementucci et al. (2023b) identified a phase of surface uplift in the Massif Central preceding the regional deep-mantle-related uplift (Babault et al., 2008). This phase may have started in the early Miocene, with ~400 m of surface uplift that is interpreted to reflect crustal-scale processes (e.g., magma injection or mantle delamination; Clementucci et al., 2023b). An alternative possibility is considering a flexural component contributing the total uplift. Given the regional tectonic context of the Massif Central, which is situated to the south of the flexural Rharb and Saiss foredeep basins (Fig. 14; Chalouan et al., 2008; Flinch, 1994), a forebulge flexural uplift related to loading in the Rif Belt may have been a contributing driving mechanism for this phase of surface uplift in the Massif Central. Forebulge uplift due to the tectonic overburden of Rif Cordillera is also recognized in the southern Rharb shelf (Le Roy et al., 2014) and supported by independent evidence such as the flexural extension in the Rharb basin (Zouhri et al., 2002) and the recent extensional deformation in the Rharb-Saiss basins coeval with compression in the Western Meseta (Bargach et al., 2004). Furthermore, flexural uplift in the Massif Central likely began during the middle-late Miocene, given the initiation of subsidence in the foredeep during this

https://doi.org/10.5194/egusphere-2024-1746
Preprint. Discussion started: 20 August 2024

time (Chalouan et al., 2008). Forebulge uplift has been demonstrated as one of the mechanisms driving topographic rejuvenation across various forelands worldwide (*e.g.,* Expósito et al., 2022; Nivière et al., 2013; Repasch et al., 2023). Typically, the amplitude of forebulge uplift is 4% to 7% of foredeep maxima (Decelles, 2012). Considering the mean of these percentages (5.5%) and a maximum of 2000m for thickness of the Saiss foredeep (Sani et al., 2007), the amplitude of the forebulge uplift in the Massif Central would be 110 m. This value is consistent with the incision heights measured in the Masssif Central (Table 1) and near to the predicted forebulge uplift (174 m) in the Sierra Morena at the foreland of the Betic Cordilleras (Garcia-Castellanos et al., 2002), which are the northern limp of Gibraltar Arc. However this estimated forebulge uplift (110 m) cannot solely account for the high elevation of Massif Central and is inconsistent with the values of surface uplift (400 m) estimated from river profiles projections for the same area (Clementucci et al., 2023b). Therefore, we suggest that the lithospheric flexure may have facilitated inflow of asthenospheric material from the adjacent Middle Atlas towards the Massif Central during the Quaternary (Fig. 14), thereby contributing to localized dynamic topography (*e.g.* Miller and Becker, 2014). This hypothesis finds support in the fact that the alkaline volcanism, associated with mantle dynamics, started in the Middle Atlas before beginning in the Massif Central (El Azzouzi et al., 2010; Rachdi, 1995). Moreover, a late Pliocene loss in the drainage area of the Bou Regreg River decreased erosion efficiency in the Massif Central, preventing it from keeping pace with the sustained uplift. This likely fostered localized surface uplift in the Massif Central (Yaaqoub and Essaifi, 2023). Therefore, the relatively high, post-lava emplacement incision rates in the Massif Central could be the result of an incision wave that migrated upstream from the Atlantic Ocean in response to flexural surface uplift.

5.4. Quaternary Landscape evolution

The Quaternary fluvial incision rates of the Middle Atlas and the Massif Central allow us to constrain the amount of relief generated in this region during the Quaternary and to gain insights into the landscape evolution before and after the lava flows emplacement. River incision rates in lava-filled valleys in the Middle Atlas range between 8 and 38 m/Ma, (i.e., only a few tens of meters in a million year),

https://doi.org/10.5194/egusphere-2024-1746
Preprint. Discussion started: 20 August 2024

whereas up to one hundred meters of fluvial incision for the same time frame is calculated for the Massif Central. This indicates that the post-lava emplacement incision in the Middle Atlas has been a relatively slow process during the Quaternary. This inference is reflected in the regional landscape when we consider the amount of relief generated after lava emplacement compared to the total relief of lava-filled valleys. Overall, the post-eruption incision represents only a small proportion of the total fluvial incision (Fig. 12, 13 A and C). Consequently, the calculated post-lava emplacement incision rates indicate that the greatest part of topographic relief in the Middle Atlas predates the Quaternary. For instance, lacustrine deposits attributed to the Mio-Pliocene (Beaudet, 1969) have undergone substantial erosion that led to their preservation in the form of buttes dispersed throughout the western boundary of the Middle Atlas where their heights reach hundreds of meters. Importantly, this significant erosion occurred before the emplacement of Quaternary lava flows (Fig. 12). Similar buttes topped by lacustrine and continental sediments shaped before the emplacement of Quaternary lavas are also observed in headwaters of the Bou Regreg catchment (Yaaqoub and Essaifi, 2023). Furthermore, a petrified lava cascade has been described at the transition by Martin (1981) between the TMA and the Western Meseta (Fig. 12 C), indicating the control of preexisting relief on the Quaternary lava flows emplacement.

https://doi.org/10.5194/egusphere-2024-1746
Preprint. Discussion started: 20 August 2024

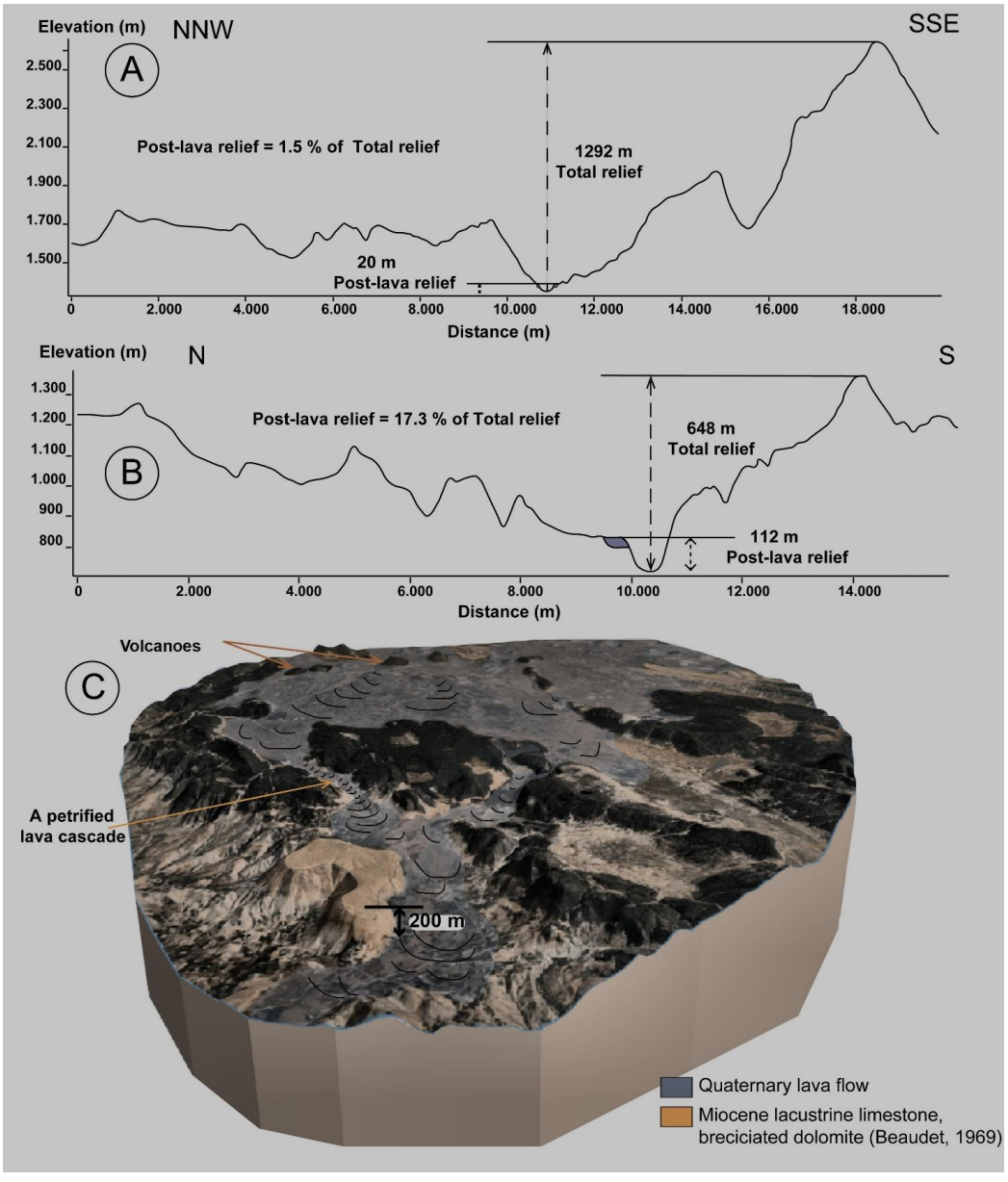

Figure 12A) and B) Cross-valley topographic profiles highlighting the total and Post lava emplacement topographic relief in the Middle Atlas and Western Meseta respectively. C) Perspective view showing the control of preexisting relief on lava flow emplacement.

662

https://doi.org/10.5194/egusphere-2024-1746
Preprint. Discussion started: 20 August 2024

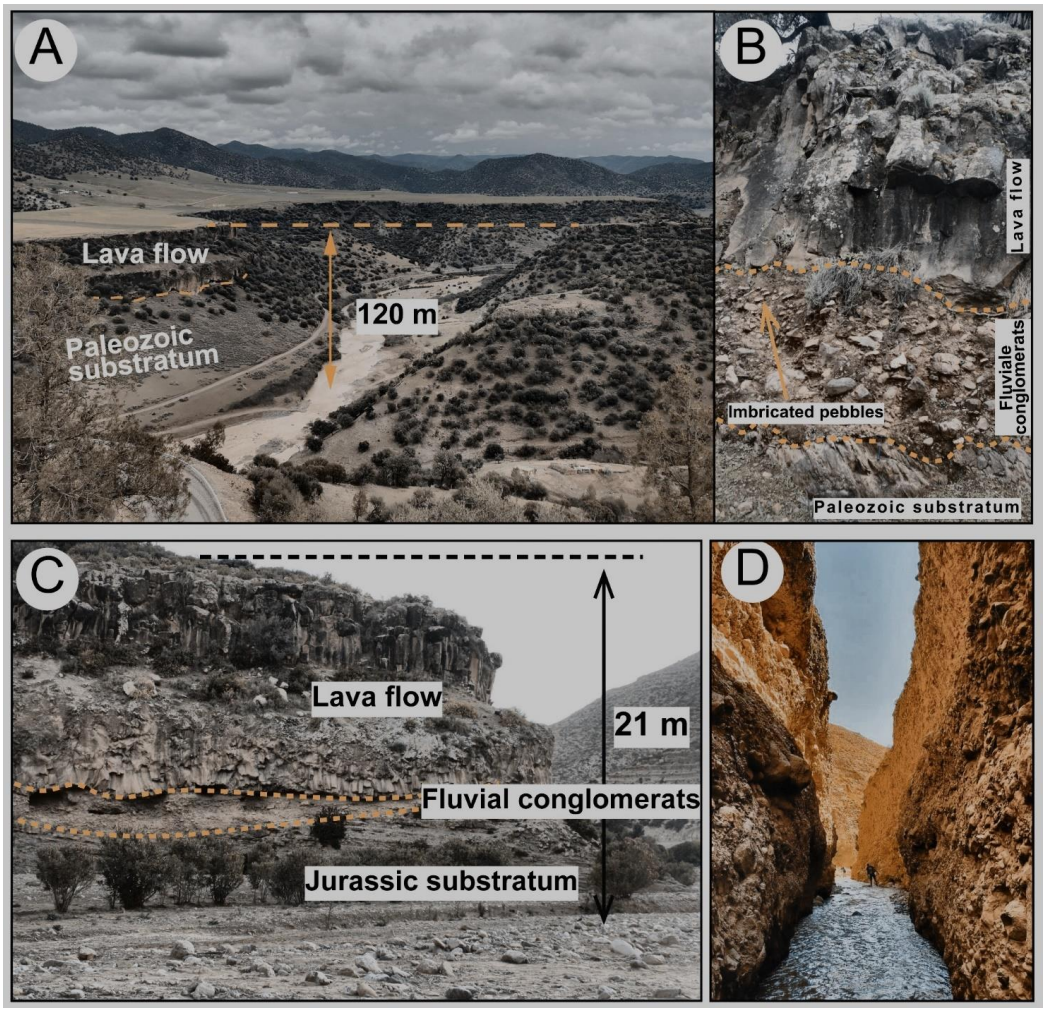

Figure 13: Field Photographs, A) landscape around Bou Tsaggatine locality, B) Left valley side at the Bled Belmadi locality showing a succession of Paleozoic basement, fluvial conglomerates, and lava flow, C) Right valley side at Taghazout locality with Jurassic substratum, fluvial conglomerates and lava flow, D) Gorges of Cheg El Ard River in the eastern flank of the Middle Atlas.

663

https://doi.org/10.5194/egusphere-2024-1746
Preprint. Discussion started: 20 August 2024

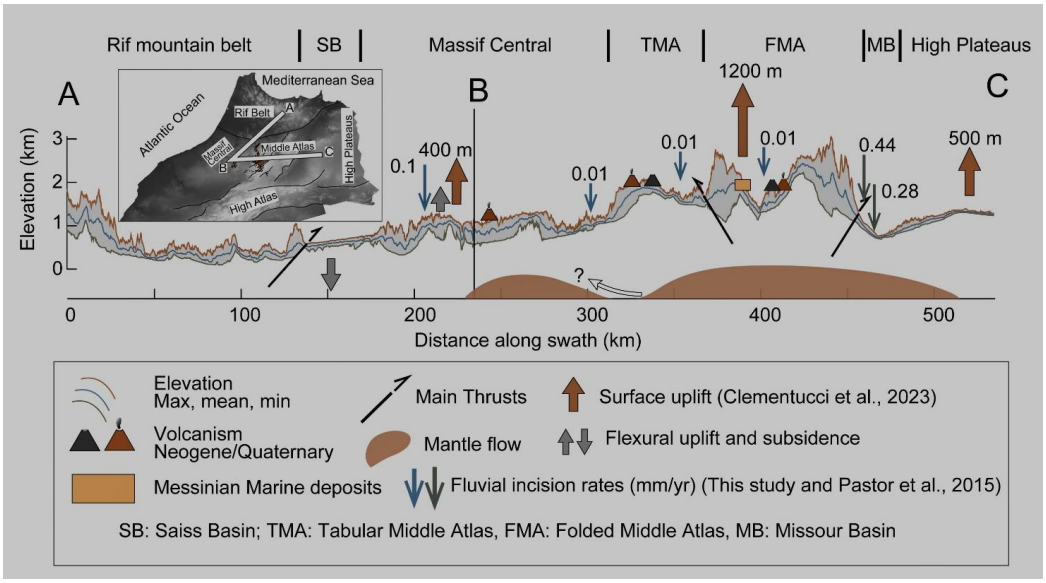

Figure 14: Schematic topographic swath profile summarizing the main data on surface uplift and incision rates across the study area. The inset shows the swath location.

6. Conclusion

The Quaternary fluvial incision rates in the Middle Atlas and the Massif Central inferred from lava flows, combined with geomorphic analysis, provide insights into the regional evolution of the geomorphic processes and the uplift history. The observed spatial discrepancy in incision rates, with values of approximately 0.01 in the Middle Atlas and 0.1 in the Massif Central, is consistent with variations in geomorphic metrics such as local relief, *Ksn*, and hypsometry. These metrics indicate higher geomorphic complexity in the Massif Central as compared to the Middle Atlas. Furthermore, a comparison of our incision rates with previously published fluvial incision rates in the northeastern flank of the Middle Atlas, suggests a dichotomy in the tectonic evolution of the Middle Atlas range with its eastern flank that is primarily accommodating active tectonic processes.

https://doi.org/10.5194/egusphere-2024-1746
Preprint. Discussion started: 20 August 2024

The calculated fluvial incision rates do not appear to be influenced by lithology or climate. Instead, the spatial distribution of surface uplift inferred from river projection in previous studies seems to strongly influence the spatial variations in fluvial incision rates. Specifically higher Quaternary incision rates are systematically downstream of major non-lithological knickpoints indicating that the elevated upstream portions of the landscape have not yet adjusted to an acceleration in surface uplift rates. High fluvial incision rates in the Moroccan Massif Central can be related to surface uplift due to the flexural uplift as a forebulge in the foreland of the Rif Belt, enhanced by the deep mantle-related uplift. These findings contribute to our understanding of the geomorphic and tectonic dynamics in the Middle Atlas and Western Meseta regions during the Quaternary and highlight the importance of lava flows as geomorphic markers.

Author contributions

AY and AE Conceptualized the study and collected the data. AY analysed the data and wrote the original draft. AE, RC, PB, RZ, CF and CP discussed the findings, reviewed and edited the manuscript.

Competing interests

The authors declare that they have no conflict of interest.

Acknowledgements

This work is part of a PhD program. The PhD student, AY, acknowledges the Moroccan National Center for Scientific and Technical Research (CNRST) for awarding him a scholarship (21UCA2019). (…)

References

Agharroud, K., Siame, L. L., Ben Moussa, A., Bellier, O., Guillou, V., Fleury, J., and El Kharim, Y.: Seismo-Tectonic Model for the Southern Pre-Rif Border (Northern Morocco): Insights From Morphochronology, Tectonics, 40, 1–24, https://doi.org/10.1029/2020TC006633, 2021.

Ahnert, F.: Functional relationships between denudation, relief, and uplift in large, mid-latitude drainage

https://doi.org/10.5194/egusphere-2024-1746
Preprint. Discussion started: 20 August 2024

699 basins, Am. J. Sci., 268, 243–263, https://doi.org/10.2475/ajs.268.3.243, 1970.

700 Allen, M. B., Mark, D. F., Kheirkhah, M., Barfod, D., Emami, M. H., and Saville, C.: 40Ar/39Ar dating of
701 Quaternary lavas in northwest Iran: Constraints on the landscape evolution and incision rates of the
702 Turkish-Iranian plateau, Geophys. J. Int., 185, 1175–1188, https://doi.org/10.1111/j.1365-
703 246X.2011.05022.x, 2011.

704 Amine, A., El Amrani El Hassani, I.-E., Remmal, T., El Kamel, F., Van Wyk De Vries, B., and Boivin, P.:
705 Geomorphological Classification and Landforms Inventory of the Middle-Atlas Volcanic Province (Morocco):
706 Scientific Value and Educational Potential, Quaest. Geogr., 38, 107–129, https://doi.org/10.2478/quageo-
707 2019-0010, 2019.

708 El Arabi, H., Ouahhabi, B., and CHarrière, A.: Les séries du Toarcien-Aalénien du SW du Moyen-Atlas
709 (Maroc): précisions stratigraphiques et signification paléogéographique, 2001.

710 Arboleya, M. L., Teixell, A., Charroud, M., and Julivert, M.: A structural transect through the High and
711 Middle Atlas of Morocco, J. African Earth Sci., 39, 319–327,
712 https://doi.org/10.1016/j.jafrearsci.2004.07.036, 2004.

713 Ayarza, P., Carbonell, R., Teixell, A., Palomeras, I., Martí, D., Kchikach, A., Harnafi, M., Levander, A., Gallart,
714 J., Arboleya, M. L., Alcalde, J., Fernández, M., Charroud, M., and Amrhar, M.: Crustal thickness and velocity
715 structure across the Moroccan Atlas from long offset wide-angle reflection seismic data: The SIMA
716 experiment, Geochemistry, Geophys. Geosystems, 15, 1698–1717,
717 https://doi.org/10.1002/2013GC005164, 2014.

718 El Azzab, D. and El Wartiti, M. E.: Paleomagnetisme des laves du Moyen Atlas (Maroc): Rotations recentes,
719 Comptes Rendus l'Academie Sci. - Ser. IIa Sci. la Terre des Planetes, 327, 509–512,
720 https://doi.org/10.1016/S1251-8050(99)80031-7, 1998.

721 El Azzouzi, M., Bernard-Griffiths, J., Bellon, H., Maury, R. C., Piqué, A., Fourcade, S., Cotten, J. ´, and
722 Hernandez, J.: Evolution of the sources of Moroccan volcanism during the Neogene, C. R. Acad. Sci., 95–

https://doi.org/10.5194/egusphere-2024-1746
Preprint. Discussion started: 20 August 2024

723 102, 1999.

724 El Azzouzi, M., Maury, R. C., Bellon, H., Youbi, N., Cotten, J., and Kharbouch, F.: Petrology and K-Ar
725 chronology of the Neogene-Quaternary Middle Atlas basaltic province, Morocco, Bull. la Soc. Geol. Fr., 181,
726 243–257, https://doi.org/10.2113/gssgfbull.181.3.243, 2010.

727 Babault, J., Teixell, A., Arboleya, M. L., and Charroud, M.: A late Cenozoic age for long-wavelength surface
728 uplift of the Atlas Mountains of Morocco, Terra Nov., 20, 102–107, https://doi.org/10.1111/j.1365-
729 3121.2008.00794.x, 2008a.

730 Babault, J., Teixell, A., Arboleya, M. L., and Charroud, M.: A late Cenozoic age for long-wavelength surface
731 uplift of the Atlas Mountains of Morocco, Terra Nov., 20, 102–107, https://doi.org/10.1111/j.1365-
732 3121.2008.00794.x, 2008b.

733 Ballato, P., Landgraf, A., Schildgen, T. F., Stockli, D. F., Fox, M., Ghassemi, M. R., Kirby, E., and Strecker, M.
734 R.: The growth of a mountain belt forced by base-level fall: Tectonics and surface processes during the
735 evolution of the Alborz Mountains, N Iran, Earth Planet. Sci. Lett., 425, 204–218,
736 https://doi.org/10.1016/j.epsl.2015.05.051, 2015.

737 Barbero, L., Jabaloy, A., Gómez-Ortiz, D., Pérez-Peña, J. V., Rodríguez-Peces, M. J., Tejero, R., Estupiñán, J.,
738 Azdimousa, A., Vázquez, M., and Asebriy, L.: Evidence for surface uplift of the Atlas Mountains and the
739 surrounding peripheral plateaux: Combining apatite fission-track results and geomorphic indicators in the
740 Western Moroccan Meseta (coastal Variscan Paleozoic basement), Tectonophysics, 502, 90–104,
741 https://doi.org/10.1016/j.tecto.2010.01.005, 2011.

742 Barcos, L., Jabaloy, A., Azdimousa, A., Asebriy, L., Gómez-Ortiz, D., Rodríguez-Peces, M. J., Tejero, R., and
743 Pérez-Peña, J. V.: Study of relief changes related to active doming in the eastern Moroccan Rif (Morocco)
744 using geomorphological indices, J. African Earth Sci., 100, 493–509,
745 https://doi.org/10.1016/j.jafrearsci.2014.07.014, 2014.

746 Bargach, K., Ruano, P., Chabli, A., Galindo-Zaldivar, J., Chalouan, A., Jabaloy, A., Akil, M., Ahmamou, M., De

https://doi.org/10.5194/egusphere-2024-1746
Preprint. Discussion started: 20 August 2024

747 Galdeano Sanz, C., and Benmakhlouf, M.: Recent tectonic deformations and stresses in the frontal part of
748 the Rif Cordillera and the Saïss basin (Fes and Rabat regions, Morocco), Pure Appl. Geophys., 161, 521–540,
749 https://doi.org/10.1007/s00024-003-2461-6, 2004.

750 Baudin, T., Chevremont, P., Razin, P., Thieblemont, D., Rachdi, H. E.-N., Roger, J., Benhaourch, R., and
751 Winckel, A.: Carte Géologique du Maroc au 1/50000. Feuille d'Oulmès - mèmoire explicatif, Notes Mém.
752 Serv. Cart. géol. Maroc N° 410bis, 2001.

753 Beauchamp, W., Barazangi, M., Demnati, A., and El Alji, M.: Intracontinental rifting and inversion: Missour
754 basin and Atlas mountains, Morocco, Am. Assoc. Pet. Geol. Bull., 80, 1459–1482,
755 https://doi.org/10.1306/64ed9a60-1724-11d7-8645000102c1865d, 1996.

756 Beaudet, G.: Le plateau central marocain et ses bordures, étude géomorphologique (bordure sud-ouest et
757 sud du plateau central), Thèse de D., Thèse Lett, Rabat, 487 pp., 1969.

758 Berrahma, M.: Etude pétrologique des laves récentes du massif du Siroua (Anti-Atlas, Maroc), Notes
759 Mémoires du Serv. géologique du Maroc, 119, 1995.

760 Bonnet, S.: Shrinking and splitting of drainage basins in orogenic landscapes from the migration of themain
761 drainage divide, Nat. Geosci., 2, 766–771, https://doi.org/10.1038/ngeo666, 2009.

762 Van Den Bosch, J. W. H.: Mémoire explicatif de la carte gravimétrique du Maroc (provinces du Nord) au
763 1/500 000, Notes Mémoires du Serv. Geol. du Maroc, 220, 1971.

764 Bouhdadi, S., Boursoumi, A. E., Chenakeb, M., Tayeb, M., and Laamayem, F.: Carte géologique Maroc
765 (1/50000), feuille Tifoughaline, 2002.

766 Boulton, S. J.: Geomorphic Response to Differential Uplift: River Long Profiles and Knickpoints From
767 Guadalcanal and Makira (Solomon Islands), Front. Earth Sci., 8, https://doi.org/10.3389/feart.2020.00010,
768 2020a.

769 Boulton, S. J.: Geomorphic Response to Differential Uplift: River Long Profiles and Knickpoints From

https://doi.org/10.5194/egusphere-2024-1746
Preprint. Discussion started: 20 August 2024

770 Guadalcanal and Makira (Solomon Islands), Front. Earth Sci., 8, https://doi.org/10.3389/feart.2020.00010,
771 2020b.

772 Boumir, K., Ouarhache, D., Feist, M., Oussou, A., Ech-charay, K., Ouaskou, M., and Charrière, A.: First
773 evidence of the Upper Jurassic deposits in the Middle Atlas (Marmoucha syncline, Morocco) and
774 connections to the Tethyan Domain, Palaeobiodiversity and Palaeoenvironments,
775 https://doi.org/10.1007/s12549-023-00593-z, 2023.

776 Brahim, L. A., Chotin, P., Hinaj, S., Abdelouafi, A., and Adraoui, A. El: Paleostress evolution in the Moroccan
777 African margin from Triassic to Present, 357, 187–205, 2002.

778 Bridgland, D. R. and Westaway, R.: Quaternary fluvial archives and landscape evolution: A global synthesis,
779 Proc. Geol. Assoc., 125, 600–629, https://doi.org/10.1016/j.pgeola.2014.10.009, 2014.

780 Burbank, D. W. and Anderson, R. S.: Rates of Erosion and Uplift, Tecton. Geomorphol., 195–242,
781 https://doi.org/10.1002/9781444345063.ch7, 2011.

782 Campforts, B., Vanacker, V., Herman, F. d. ri., Vanmaercke, M., Schwanghart, W., Tenorio, G. E., Willems, P.,
783 and Govers, G.: Parameterization of river incision models requires accounting for environmental
784 heterogeneity: Insights from the tropical Andes, Earth Surf. Dyn., 8, 447–470,
785 https://doi.org/10.5194/esurf-8-447-2020, 2020.

786 Chalouan, A., Michard, A., Kadiri, K. El, Negro, F., Lamotte, D. F. de, Soto, J. I., and Saddiqi, O.: The Rif Belt,
787 in: Continental Evolution: The Geology of Morocco: Structure, Stratigraphy, and Tectonics of the Africa-
788 Atlantic-Mediterranean Triple Junction, edited by: Michard, A., Saddiqi, O., Chalouan, A., and Lamotte, D. F.
789 de, Springer Berlin Heidelberg, Berlin, Heidelberg, 203–302, https://doi.org/10.1007/978-3-540-77076-3_5,
790 2008.

791 Champagnac, J., Molnar, P., Sue, C., and Herman, F.: Tectonics, climate, and mountain topography, J.
792 Geophys. Res. Solid Earth, 117, https://doi.org/10.1029/2011JB008348, 2012.

793 Charriere, A.: Evolution neogene de bassins continentaux et marins dans le Moyen Atlas central (Maroc),

https://doi.org/10.5194/egusphere-2024-1746
Preprint. Discussion started: 20 August 2024

794 Bull. la Société Géologique Fr., S7-XXVI, 1127–1136, https://doi.org/10.2113/gssgfbull.S7-XXVI.6.1127,
795 1984.

796 Charrière, A.: Héritage hercynien et évolution géodynamique alpine d'une chaîne intracontinentale: le
797 Moyen Atlas au SE de Fès (Maroc), Paul-Sabatier de Toulouse III, 589 pp., 1990.

798 Charrière, A., Du Dresnay, R., and Izart, A.: Quantitative evaluation of subsidence during Lower and Middle
799 Jurassic times in the Middle Atlas Basin, Morocco, Comptes Rendus - Acad. des Sci. Ser. II Sci. la Terre des
800 Planetes, 318, 829–835, 1994.

801 Clementucci, R., Ballato, P., Siame, L. L., Faccenna, C., Yaaqoub, A., Essaifi, A., Leanni, L., and Guillou, V.:
802 Lithological control on topographic relief evolution in a slow tectonic setting (Anti-Atlas, Morocco), Earth
803 Planet. Sci. Lett., 596, https://doi.org/10.1016/j.epsl.2022.117788, 2022a.

804 Clementucci, R., Ballato, P., Siame, L. L., Faccenna, C., Yaaqoub, A., Essaifi, A., Leanni, L., and Guillou, V.:
805 Lithological control on topographic relief evolution in a slow tectonic setting (Anti-Atlas, Morocco), Earth
806 Planet. Sci. Lett., 596, 117788, https://doi.org/10.1016/j.epsl.2022.117788, 2022b.

807 Clementucci, R., Ballato, P., Siame, L., Fox, M., Lanari, R., Sembroni, A., Faccenna, C., Yaaqoub, A., and
808 Essaifi, A.: Surface Uplift and Topographic Rejuvenation of a Tectonically Inactive Range: Insights From the
809 Anti-Atlas and the Siroua Massif (Morocco), Tectonics, 42, https://doi.org/10.1029/2022TC007383, 2023a.

810 Clementucci, R., Ballato, P., Siame, L. L., Faccenna, C., Racano, S., Torreti, G., Lanari, R., Leanni, L., and
811 Guillou, V.: Transient response to changes in uplift rates in the northern Atlas-Meseta system (Morocco),
812 Geomorphology, 436, 108765, https://doi.org/10.1016/j.geomorph.2023.108765, 2023b.

813 Colo, G.: Contribution à l'étude du Jurassique du Moyen atlas septentrional, Notes et Mémoires du Service
814 Géologique du Maroc. 139, 226 pp., 1961.

815 Crosby, B. T. and Whipple, K. X.: Knickpoint initiation and distribution within fluvial networks: 236 waterfalls
816 in the Waipaoa River, North Island, New Zealand, Geomorphology, 82, 16–38,
817 https://doi.org/10.1016/j.geomorph.2005.08.023, 2006.

https://doi.org/10.5194/egusphere-2024-1746
Preprint. Discussion started: 20 August 2024

818 Decelles, P. G.: Foreland Basin Systems Revisited: Variations in Response to Tectonic Settings, Tectonics
819 Sediment. Basins Recent Adv., 405–426, https://doi.org/10.1002/9781444347166.ch20, 2012.

820 Delcaillau, B., Laville, E., Carozza, J. M., Dugué, O., Charroud, M., and Amrhar, M.: Morphotectonic
821 evolution of the Jebel Bou Naceur in the South Middle Atlas Fault Zone (Morocco), Comptes Rendus -
822 Geosci., 339, 553–561, https://doi.org/10.1016/j.crte.2007.06.005, 2007.

823 Demir, T., Westaway, R., Bridgland, D., Pringle, M., Yurtmen, S., Beck, A., and Rowbotham, G.: Ar-Ar dating
824 of late Cenozoic basaltic volcanism in northern Syria: Implications for the history of incision by the River
825 Euphrates and uplift of the northern Arabian Platform, Tectonics, 26, 1–30,
826 https://doi.org/10.1029/2006TC001959, 2007.

827 Demoulin, A., Mather, A., and Whittaker, A.: Fluvial archives, a valuable record of vertical crustal
828 deformation, Quat. Sci. Rev., 166, 10–37, https://doi.org/10.1016/j.quascirev.2016.11.011, 2017.

829 Du Dresnay, R.: Recent Data on the geology of the Middle-Atlas (Morocco), JACOBSHACEN. V. (ed.)The Atlas
830 Syst. Morocco. Springer-Verlag. Berlin, 293–320, 1988.

831 England, P. and Molnar, P.: Surface uplift, uplift of rocks, and exhumation of rocks, Geology, 18, 1173–1177,
832 https://doi.org/10.1130/0091-7613(1990)018<1173:SUUORA>2.3.CO;2, 1990.

833 Essaifi, A., Samson, S., and Goodenough, K.: Geochemical and Sr–Nd isotopic constraints on the
834 petrogenesis and geodynamic significance of the Jebilet magmatism (Variscan Belt, Morocco), Geol. Mag.,
835 151, 666–691, https://doi.org/10.1017/S0016756813000654, 2014.

836 Evenstar, L. A., Mather, A. E., and Hartley, A. J.: Using spatial patterns of fluvial incision to constrain
837 continental-scale uplift in the Andes, Glob. Planet. Change, 186, 103119,
838 https://doi.org/10.1016/j.gloplacha.2020.103119, 2020.

839 Expósito, I., Jiménez-Bonilla, A., Delchiaro, M., Yanes, J. L., Balanyá, J. C., Moral-Martos, F., and Della Seta,
840 M.: Geomorphic signature of segmented relief rejuvenation in the Sierra Morena, Betic forebulge, Spain,
841 Earth Surf. Dyn., 10, 1017–1039, https://doi.org/10.5194/esurf-10-1017-2022, 2022.

https://doi.org/10.5194/egusphere-2024-1746
Preprint. Discussion started: 20 August 2024

842 Fedan, B.: Evolution géodynamique d'un bassin intraplaque sur décrochements: Le Moyen Atlas (Maroc)
843 durant le Méso-Cénozoique, La faculté des sciences de rabat, université mohammed V, 144 pp., 1988.

844 Fedan, B. and Thomas, G.: Découverte de dépôts néogènes déformés par l'accident nord-moyen atlasique
845 (Maroc). Implications sur son activité mio-plio-quaternaire au Nord de Boulemane, Géologie
846 Méditerranéenne, 12, 151–154, https://doi.org/10.3406/geolm.1985.1345, 1985.

847 Fekkak, A., Ouanaimi, H., Michard, A., Soulaimani, A., Ettachfini, E. M., Berrada, I., El Arabi, H., Lagnaoui, A.,
848 and Saddiqi, O.: Thick-skinned tectonics in a Late Cretaceous-Neogene intracontinental belt (High Atlas
849 Mountains, Morocco): The flat-ramp fault control on basement shortening and cover folding, J. African
850 Earth Sci., 140, 169–188, https://doi.org/10.1016/j.jafrearsci.2018.01.008, 2018.

851 Ferrier, K. L., Huppert, K. L., and Perron, J. T.: Climatic control of bedrock river incision, Nature, 496, 206–
852 209, https://doi.org/10.1038/nature11982, 2013.

853 Flinch, J. F.: Tectonic evolution of the Gibraltar Arc, https://hdl.handle.net/1911/16726., 1994.

854 Forte, A. M. and Whipple, K. X.: Short communication: The Topographic Analysis Kit (TAK) for TopoToolbox,
855 Earth Surf. Dyn., 7, 87–95, https://doi.org/10.5194/esurf-7-87-2019, 2019.

856 Frizon de Lamotte, D., Saint Bezar, B., Bracène, R., and Mercier, E.: The two main steps of the Atlas building
857 and geodynamics of the western Mediterranean, Tectonics, 19, 740–761,
858 https://doi.org/10.1029/2000TC900003, 2000.

859 Frizon de Lamotte, D., Leturmy, P., Missenard, Y., Khomsi, S., Ruiz, G., Saddiqi, O., Guillocheau, F., and
860 Michard, A.: Mesozoic and Cenozoic vertical movements in the Atlas system (Algeria, Morocco, Tunisia): An
861 overview, Tectonophysics, 475, 9–28, https://doi.org/10.1016/j.tecto.2008.10.024, 2009.

862 Frizon De Lamotte, D., Zizi, M., Missenard, Y., Hafid, M., El Azzouzi, M., Maury, R. C., Charrière, A., Taki, Z.,
863 Benammi, M., and Michard, A.: The Atlas system, Lect. Notes Earth Sci., 116, 133–202,
864 https://doi.org/10.1007/978-3-540-77076-3_4, 2008.

https://doi.org/10.5194/egusphere-2024-1746
Preprint. Discussion started: 20 August 2024

865 Fullea, J., Fernàndez, M., Afonso, J. C., Vergés, J., and Zeyen, H.: The structure and evolution of the
866 lithosphere-asthenosphere boundary beneath the Atlantic-Mediterranean Transition Region, Lithos, 120,
867 74–95, https://doi.org/10.1016/j.lithos.2010.03.003, 2010.

868 Fuller, T. K., Perg, L. A., Willenbring, J. K., and Lepper, K.: Field evidence for climate-driven changes in
869 sediment supply leading to strath terrace formation, Geology, 37, 467–470,
870 https://doi.org/10.1130/G25487A.1, 2009.

871 Gallen, S. F. and Wegmann, K. W.: River profile response to normal fault growth and linkage: An example
872 from the Hellenic forearc of south-central Crete, Greece, Earth Surf. Dyn., 5, 161–186,
873 https://doi.org/10.5194/esurf-5-161-2017, 2017.

874 Garcia-Castellanos, D., Fernàndez, M., and Torne, M.: Modeling the evolution of the Guadalquivir foreland
875 basin (southern Spain), Tectonics, 21, 9-1-9–17, https://doi.org/10.1029/2001TC001339, 2002.

876 Ghorbal, B., Bertotti, G., Foeken, J., and Andriessen, P.: Unexpected Jurassic to Neogene vertical
877 movements in 'stable'parts of NW Africa revealed by low temperature geochronology, Terra Nov., 20, 355–
878 363, https://doi.org/10.1111/j.1365-3121.2008.00828.x, 2008.

879 Gomez, F., Allmendinger, R., Barazangi, M., Er-Raji, A., and Dahmani, M.: Crustal shortening and vertical
880 strain partitioning in the Middle Atlas Mountains of Morocco, Tectonics, 17, 520–533,
881 https://doi.org/10.1029/98TC01439, 1998a.

882 Gomez, F., Allmendinger, R. W., Barazangi, M., Er-raji, A., and Dahmani, M.: Crustal shortening and vertical
883 strain partitioning tabular regions of, Tectonics, 17, 520–533, 1998b.

884 Gomez, F., Barazangi, M., and Demnati, A.: Structure and Evolution of the Neogene Guercif Basin at the
885 Junction of the Middle Atlas Mountains and the Rif Thrust Belt, Morocco, Am. Assoc. Pet. Geol. Bull., 84,
886 1340–1364, https://doi.org/10.1306/a9673ea0-1738-11d7-8645000102c1865d, 2000.

887 Gomez Francisco, B. M. & B. M.: Active tectonism in the intracontinental Middle Atlas Mountains of
888 Morocco : synchronous crustal shortening and extension, J. Geol. Soc. London, 153, 389–402, 1996.

https://doi.org/10.5194/egusphere-2024-1746
Preprint. Discussion started: 20 August 2024

889 Harmand, C. and Cantagrel, J. M.: Le volcanisme alcalin tertiaire et quaternaire du moyen atlas (Maroc):
890 chronologie K/Ar et cadre géodynamique, J. African Earth Sci., 2, 51–55, https://doi.org/10.1016/0899-
891 5362(84)90019-8, 1984.

892 Harris, I., Osborn, T. J., Jones, P., and Lister, D.: Version 4 of the CRU TS monthly high-resolution gridded
893 multivariate climate dataset, Sci. Data, 7, 1–18, https://doi.org/10.1038/s41597-020-0453-3, 2020.

894 Hartshorn, K., Hovius, N., Dade, W. B., and Slingerland, R. L.: Climate-driven bedrock incision in an active
895 mountain belt, Science (80-.)., 297, 2036–2038, https://doi.org/10.1126/science.1075078, 2002.

896 Hinaje, S., Fartati, M. El, Yaagoub, D., Amrani, S., Gharmane, Y., and Idrissi, B. E. F.: Paleocontraintes et
897 Contexte Tectonique de Mise en Place du Volcanisme Alcalin Neogene et Quaternaire du Moyen Atlas
898 (Maroc), Eur. Sci. J. ESJ, 15, 448–466, https://doi.org/10.19044/esj.2019.v15n15p448, 2019.

899 Hoepffner, C., Soulaimani, A., and Piqué, A.: The Moroccan Hercynides, J. African Earth Sci., 43, 144–165,
900 https://doi.org/10.1016/j.jafrearsci.2005.09.002, 2005.

901 Howard, A. D. and Kerby, G.: Channel ch ages in badlands, Geol. Soc. Am. Bull., 94, 739–752, 1983.

902 Jacobshagen V., G. K. & G. P.: Geodynamic evolution of the Atlas System (Morocco) in post-Palaeozoic
903 times., in: JACOBSHAGEN, V. (ed.) The Atlas System of Morocco., vol. 15, edited by: Springer-Verlag, Berlin,
904 481–499, 1988.

905 Jaiswara, N. K., Kotluri, S. K., Pandey, P., and Pandey, A. K.: MATLAB functions for extracting hypsometry,
906 stream-length gradient index, steepness index, chi gradient of channel and swath profiles from digital
907 elevation model (DEM) and other spatial data for landscape characterisation, Appl. Comput. Geosci., 7,
908 100033, https://doi.org/10.1016/j.acags.2020.100033, 2020.

909 Keller, E. A. and Pinter, N.: Active Tectonics, 2nd ed., 383 pp., 2002.

910 Kirby, E. and Whipple, K. X.: Expression of active tectonics in erosional landscapes, J. Struct. Geol., 44, 54–
911 75, https://doi.org/10.1016/j.jsg.2012.07.009, 2012a.

https://doi.org/10.5194/egusphere-2024-1746
Preprint. Discussion started: 20 August 2024

912 Kirby, E. and Whipple, K. X.: Expression of active tectonics in erosional landscapes,
913 https://doi.org/10.1016/j.jsg.2012.07.009, November 2012b.

914 Kuhni, A. and Pfiffner, O. A.: The relief of the Swiss Alps and adjacent areas and its relation to lithology and
915 structure: topographic analysis from a 250-m DEM, Geomorphology, 285–307 pp., 2001.

916 Lague, D.: The stream power river incision model: Evidence, theory and beyond, Earth Surf. Process.
917 Landforms, 39, 38–61, https://doi.org/10.1002/esp.3462, 2014.

918 Lanari, R., Faccenna, C., Fellin, M. G., Essaifi, A., Nahid, A., Medina, F., and Youbi, N.: Tectonic Evolution of
919 the Western High Atlas of Morocco: Oblique Convergence, Reactivation, and Transpression, Tectonics, 39,
920 https://doi.org/10.1029/2019TC005563, 2020.

921 Lanari, R., Reitano, R., Giachetta, E., Pazzaglia, F. J., Clementucci, R., Faccenna, C., and Fellin, M. G.: Is the
922 Anti-Atlas of Morocco still uplifting?, J. African Earth Sci., 188,
923 https://doi.org/10.1016/j.jafrearsci.2022.104481, 2022.

924 Lanari, R., Boutoux, A., Faccenna, C., Herman, F., Willett, S. D., and Ballato, P.: Cenozoic exhumation in the
925 Mediterranean and the Middle East, Earth-Science Rev., 237, 104328,
926 https://doi.org/10.1016/j.earscirev.2023.104328, 2023a.

927 Lanari, R., Faccenna, C., Natali, C., Şengül Uluocak, E., Fellin, M. G., Becker, T. W., Göğüş, O. H., Youbi, N.,
928 Clementucci, R., and Conticelli, S.: The Atlas of Morocco: A Plume-Assisted Orogeny, Geochemistry,
929 Geophys. Geosystems, 24, 1–28, https://doi.org/10.1029/2022GC010843, 2023b.

930 Lavé, J. and Avouac, J. P.: Fluvial incision and tectonic uplift across the Himalayas of central Nepal, J.
931 Geophys. Res. Solid Earth, 106, 26561–26591, https://doi.org/10.1029/2001JB000359, 2001.

932 Laville, E., Delcaillau, B., Charroud, M., Dugué, O., Ait Brahim, L., Cattaneo, G., Deluca, P., and Bouazza, A.:
933 The Plio-Pleistocene evolution of the Southern Middle Atlas fault zone (SMAFZ) front of Morocco, Int. J.
934 Earth Sci., 96, 497–515, https://doi.org/10.1007/s00531-006-0113-7, 2007.

https://doi.org/10.5194/egusphere-2024-1746
Preprint. Discussion started: 20 August 2024

Lin, L., Li, X., and Ma, Z.: Quantifying the Geomorphology of the Drainage Basins Along the Greater Khingan Mountains in NE China, Front. Earth Sci., 9, https://doi.org/10.3389/feart.2021.796610, 2021.

Makris, J., Demnati, A., and Klussmann, J.: Deep seismic soundings in Morocco and a crust and upper mantle model deduced from seismic and gravity data, in: Annales geophysicae (1983), 369–380, 1985.

Martin, J.: Le Moyen Atlas Central: étude géomorphologique, Notes Mémoires du Serv. géologique du Maroc, 70, 445, 1981.

Mattauer, M., Tapponnier, P., and Proust, F.: Sur les mecanismes de formation des chaines intracontinentales; l'exemple des chaines atlasiques du Maroc, Bull. la Société Géologique Fr., S7-XIX, 521–526, https://doi.org/10.2113/gssgfbull.s7-xix.3.521, 1977.

Michard, A.: Eléments de géologie marocaine, Notes Mém. Serv. Cart. géol. Maroc, 252, 408 p, 1976.

Michard, A., Driouch, Y., Kuiper, Y. D., Caby, R., Farah, A., Ouanaimi, H., Soulaimani, A., Chabou, M. C., and Saddiqi, O.: The Variscan belts of North-West Africa: An African legacy to the Wilson Cycle concept, J. African Earth Sci., 208, 105042, https://doi.org/10.1016/j.jafrearsci.2023.105042, 2023a.

Michard, A., Driouch, Y., Kuiper, Y. D., Caby, R., Farah, A., Ouanaimi, H., Soulaimani, A., Chabou, M. C., and Saddiqi, O.: The Variscan belts of North-West Africa: An African legacy to the Wilson Cycle concept, J. African Earth Sci., 208, 105042, https://doi.org/10.1016/j.jafrearsci.2023.105042, 2023b.

Miller, M. S. and Becker, T. W.: Reactivated lithospheric-scale discontinuities localize dynamic uplift of the Moroccan Atlas Mountains, Geology, 42, 35–38, https://doi.org/10.1130/G34959.1, 2014.

Missenard, Y., Zeyen, H., Frizon de Lamotte, D., Leturmy, P., Petit, C., Sébrier, M., and Saddiqi, O.: Crustal versus asthenospheric origin of relief of the Atlas Mountains of Morocco, J. Geophys. Res. Solid Earth, 111, 1–13, https://doi.org/10.1029/2005JB003708, 2006.

Montgomery, D. R. and Gran, K. B.: Downstream variations in the width of bedrock channels, Water Resour. Res., 37, 1841–1846, https://doi.org/10.1029/2000WR900393, 2001.

https://doi.org/10.5194/egusphere-2024-1746
Preprint. Discussion started: 20 August 2024

958 Moumeni, M., Delchiaro, M., Seta, M. Della, Nozaem, R., Ballato, P., Leonard, J. S., Clementucci, R., and
959 Rouhi, J.: Interplay between tectonics and surface processes in the evolution of mountain ranges: Insights
960 from landscape dynamics, uplift, and active deformation of Talesh Mountains (NW Iranian Plateau margin),
961 Geomorphology, 448, 109029, https://doi.org/10.1016/j.geomorph.2023.109029, 2024.

962 Mountaj, S., Remmal, T., Lakroud, K., Boivin, P., El Amrani, I. E. E. H., El Kamel, F., Makhoukhi, S., Jounaid,
963 H., Amraoui, F., and Soufi, M.: The volcanic field of the middle atlas causse: Highlights and heritage
964 appropriation, Geogr. Bull. - Gamma Theta Upsilon, 60, 127–147, 2019.

965 Nivière, B., Messager, G., Carretier, S., and Lacan, P.: Geomorphic expression of the southern Central Andes
966 forebulge (37°S, Argentina), Terra Nov., 25, 361–367, https://doi.org/10.1111/ter.12044, 2013.

967 Ott, R. F., Whipple, K. X., and van Soest, M.: Incision history of the Verde Valley region and implications for
968 uplift of the Colorado Plateau (central Arizona), Geosphere, 14, 1690–1709,
969 https://doi.org/10.1130/GES01640.1, 2018.

970 Ouanaimi, H., Soulaimani, A., Hoepffner, C., and Michard, A.: The “Eovariscan Synmetamorphic Phase” of
971 the Moroccan Meseta Domain Revisited; A Hint for Late Devonian Extensional Geodynamics Prior to the
972 Variscan Orogenic Evolution, 259–261, https://doi.org/10.1007/978-3-030-01455-1_56, 2019.

973 Palumbo, L., Hetzel, R., Tao, M., and Li, X.: Topographic and lithologic control on catchment-wide
974 denudation rates derived from cosmogenic 10Be in two mountain ranges at the margin of NE Tibet,
975 Geomorphology, 117, 130–142, https://doi.org/10.1016/j.geomorph.2009.11.019, 2010.

976 Pan, B., Geng, H., Hu, X., Sun, R., and Wang, C.: The topographic controls on the decadal-scale erosion rates
977 in Qilian Shan Mountains, N.W. China, Earth Planet. Sci. Lett., 292, 148–157,
978 https://doi.org/10.1016/j.epsl.2010.01.030, 2010.

979 Pan, B., Hu, X., Gao, H., Hu, Z., Cao, B., Geng, H., and Li, Q.: Late Quaternary river incision rates and rock
980 uplift pattern of the eastern Qilian Shan Mountain, China, Geomorphology, 184, 84–97,
981 https://doi.org/10.1016/j.geomorph.2012.11.020, 2013.

https://doi.org/10.5194/egusphere-2024-1746
Preprint. Discussion started: 20 August 2024

982 Pastor, A., Babault, J., Owen, L. A., Teixell, A., and Arboleya, M.-L.: Extracting dynamic topography from
983 river profiles and cosmogenic nuclide geochronology in the Middle Atlas and the High Plateaus of Morocco,
984 Tectonophysics, 663, 95–109, https://doi.org/10.1016/j.tecto.2015.06.007, 2015.

985 Pazzaglia, F. J.: 9.22 Fluvial Terraces, in: Treatise on Geomorphology, Elsevier, 379–412,
986 https://doi.org/10.1016/B978-0-12-374739-6.00248-7, 2013.

987 Pérez-Peña, J. V., Azañón, J. M., Azor, A., Tuccimei, P., Della Seta, M., and Soligo, M.: Quaternary landscape
988 evolution and erosion rates for an intramontane Neogene basin (Guadix–Baza basin, SE Spain),
989 Geomorphology, 106, 206–218, https://doi.org/10.1016/j.geomorph.2008.10.018, 2009.

990 Perron, J. T. and Royden, L.: An integral approach to bedrock river profile analysis, Earth Surf. Process.
991 Landforms, 38, 570–576, https://doi.org/10.1002/esp.3302, 2013.

992 Rachdi, H. E.-N.: Etude du volcanisme plio-quaternaire du Maroc central: pétrographie, géochimie et
993 minéralogie., Notes Mémoires du Serv. Geol. du Maroc, 117, 1995.

994 Reitano, R., Clementucci, R., Conrad, E. M., Corbi, F., Lanari, R., Faccenna, C., and Bazzucchi, C.: Stream laws
995 in analog tectonic-landscape models, Earth Surf. Dyn., 11, 731–740, https://doi.org/10.5194/esurf-11-731-
996 2023, 2023.

997 Repasch, M., Scheingross, J. S., Cook, K. L., Sachse, D., Dosch, S., Orfeo, O., and Hovius, N.: Lithospheric
998 Flexure Controls on Geomorphology, Hydrology, and River Chemistry in the Andean Foreland Basin, AGU
999 Adv., 4, https://doi.org/10.1029/2023AV000924, 2023.

1000 Le Roy, P., Sahabi, M., Maad, N., Rabineau, M., Gutscher, M. A., Babonneau, N., Van Vliet Lanoe, B., Ait
1001 Brahim, L., M'hammdi, N., Trentesaux, A., Dakki, M., and Hssain, M.: 3D architecture of Quaternary
1002 sediment along the NW Atlantic Moroccan Rharb continental shelf: A stratal pattern under the dual control
1003 of tectonics and climatic variations, Mar. Pet. Geol., 49, 129–142,
1004 https://doi.org/10.1016/j.marpetgeo.2013.10.003, 2014.

1005 Safran, E. B., Bierman, P. R., Aalto, R., Dunne, T., Whipple, K. X., and Caffee, M.: Erosion rates driven by

https://doi.org/10.5194/egusphere-2024-1746
Preprint. Discussion started: 20 August 2024

channel network incision in the Bolivian Andes, Earth Surf. Process. Landforms, 30, 1007–1024, https://doi.org/10.1002/esp.1259, 2005.

Sani, F., Del Ventisette, C., Montanari, D., Bendkik, A., and Chenakeb, M.: Structural evolution of the Rides Prerifaines (Morocco): structural and seismic interpretation and analogue modelling experiments, Int. J. Earth Sci., 96, 685–706, https://doi.org/10.1007/s00531-006-0118-2, 2007.

Schildgen, T. F., Hodges, K. V., Whipple, P. W., Reiners, P. W., and Pringle, M. S.: Uplift of the western margin of the Andean plateau revealed from canyon incision history, southern Peru, Geology, 35, 523–526, https://doi.org/10.1130/G23532A.1, 2007.

Schumm, S. A.: Evolution of drainage systems and slopes in badlands at perth amboy, New Jersey., Bull. Geol. Soc. Am., 67, 597–646, https://doi.org/10.1130/0016-7606(1956)67, 1956.

Schwanghart, W. and Scherler, D.: Short Communication: TopoToolbox 2 - MATLAB-based software for topographic analysis and modeling in Earth surface sciences, Earth Surf. Dyn., 2, 1–7, https://doi.org/10.5194/esurf-2-1-2014, 2014.

Siravo, G., Molin, P., Sembroni, A., Fellin, M. G., and Faccenna, C.: Tectonically driven drainage reorganization in the Eastern Cordillera, Colombia, Geomorphology, 389, 107847, https://doi.org/10.1016/j.geomorph.2021.107847, 2021.

Sklar, L. S. and Dietrich, W. E.: Sediment and rock strength controls on river incision into bedrock, Geology, 29, 1087, https://doi.org/10.1130/0091-7613(2001)029<1087:SARSCO>2.0.CO;2, 2001.

Snyder, N. P., Whipple, K. X., Tucker, G. E., and Merritts, D. J.: Landscape response to tectonic forcing: Digital elevation model analysis of stream profiles in the Mendocino triple junction region, northern California, Geol. Soc. Am. Bull., 112, 1250–1263, https://doi.org/10.1130/0016-7606(2000)112<1250:lrttfd>2.3.co;2, 2000.

Strahler, A.: Hypsometric (area–altitude) analysis of erosional topography., Geol. Soc. Am. Bull., 63, 1117–1142, https://doi.org/10.1130/0016-7606(1952)63, 1952.

https://doi.org/10.5194/egusphere-2024-1746
Preprint. Discussion started: 20 August 2024

1030 Strahler, A.: Quantitative Analysis of Watershed Geomorphology, Transactions of the American Geophysical
1031 Union., Trans. Am. Geophys. Union, 38, 913–920, 1957.

1032 Struth, L., Giachetta, E., Willett, S. D., Owen, L. A., and Tesón, E.: Quaternary drainage network
1033 reorganization in the Colombian Eastern Cordillera plateau, Earth Surf. Process. Landforms, 45, 1789–1804,
1034 https://doi.org/10.1002/esp.4846, 2020.

1035 Tadili, B., Ramdani, M., Ben Sari, D., Chapochnikov, K., and Bellot, A.: Structure de la croûte dans le nord du
1036 Maroc, in: Annales geophysicae. Series B. Terrestrial and planetary physics, 99–104, 1986.

1037 Teixell, A., Ayarza, P., Zeyen, H., and Ferna, M.: Effects of mantle upwelling in a compressional setting : the
1038 Atlas Mountains of Morocco, https://doi.org/10.1111/j.1365-3121.2005.00633.x, 2005.

1039 Teixell, A., Bertotti, G., de Lamotte, D. F., and Charroud, M.: The geology of vertical movements of the
1040 lithosphere: An overview, Tectonophysics, 475, 1–8, https://doi.org/10.1016/j.tecto.2009.08.018, 2009.

1041 Telbisz, T., Kovács, G., Székely, B., and Szabó, J.: Topographic swath profile analysis: A generalization and
1042 sensitivity evaluation of a digital terrain analysis tool, Zeitschrift fur Geomorphol., 57, 485–513,
1043 https://doi.org/10.1127/0372-8854/2013/0110, 2013.

1044 Whipple, K. X.: The influence of climate on the tectonic evolution of mountain belts, Nat. Geosci., 2, 97–
1045 104, https://doi.org/10.1038/ngeo413, 2009.

1046 Whipple, K. X. and Tucker, G. E.: Dynamics of the stream-power river incision model: Implications for height
1047 limits of mountain ranges, landscape response timescales, and research needs, J. Geophys. Res. Solid Earth,
1048 104, 17661–17674, https://doi.org/10.1029/1999jb900120, 1999.

1049 Whipple, K. X., DiBiase, R. A., and Crosby, B. T.: 9.28 Bedrock Rivers, in: Treatise on Geomorphology,
1050 Elsevier, 550–573, https://doi.org/10.1016/B978-0-12-374739-6.00254-2, 2013.

1051 Whittaker, A. C.: How do landscapes record tectonics and climate?, Lithosphere, 4, 160–164,
1052 https://doi.org/10.1130/RF.L003.1, 2012.

https://doi.org/10.5194/egusphere-2024-1746
Preprint. Discussion started: 20 August 2024

Wigger, P., Asch, G., Giese, P., Heinsohn, W. D., Alami, S. O. el, and Ramdani, F.: Crustal structure along a traverse across the Middle and High Atlas mountains derived from seismic refraction studies, Geol. Rundschau, 81, 237–248, https://doi.org/10.1007/BF01764552, 1992.

Willett, S. D.: Orogeny and orography: The effects of erosion on the structure of mountain belts, JOURNAL OF GEOPHYSICAL RESEARCH, 957–985 pp., 1999.

Willett, S. D., Slingerland, R., and Hovius, N.: Uplift, shortening, and steady state topography in active mountain belts, Am. J. Sci., 301, 455–485, https://doi.org/10.2475/ajs.301.4-5.455, 2001.

Willett, S. D., McCoy, S. W., Taylor Perron, J., Goren, L., and Chen, C. Y.: Dynamic reorganization of River Basins, Science (80-.)., 343, https://doi.org/10.1126/science.1248765, 2014.

Winiger, M., Gumpert, M., and Yamout, H.: Karakorum–Hindukush–western Himalaya: assessing high-altitude water resources, Hydrol. Process., 19, 2329–2338, https://doi.org/10.1002/hyp.5887, 2005.

Wobus, C., Whipple, K. X., Kirby, E., Snyder, N., Johnson, J., Spyropolou, K., Crosby, B., and Sheehan, D.: Tectonics from topography: Procedures, promise, and pitfalls, Spec. Pap. Geol. Soc. Am., 398, 55–74, https://doi.org/10.1130/2006.2398(04), 2006.

Wolff, R., Hetzel, R., and Strobl, M.: Quantifying river incision into low-relief surfaces using local and catchment-wide 10Be denudation rates, Earth Surf. Process. Landforms, 43, 2327–2341, https://doi.org/10.1002/esp.4394, 2018.

Wu, D., Li, B., Lu, H., Zhao, J., Zheng, X., and Li, Y.: Spatial variations of river incision rate in the northern Chinese Tian Shan range derived from late Quaternary fluvial terraces, Glob. Planet. Change, 185, 103082, https://doi.org/10.1016/j.gloplacha.2019.103082, 2020.

Yaaqoub, A. and Essaifi, A.: Geomorphology Drainage rearrangement and landscape evolution : Insights from the Moroccan Massif Central, Geomorphology, 437, 108811, https://doi.org/10.1016/j.geomorph.2023.108811, 2023.

https://doi.org/10.5194/egusphere-2024-1746
Preprint. Discussion started: 20 August 2024

Zafaty, O., Oukassou, M., Si Mhamdi, H., Tabuce, R., and Charrière, A.: Integrated remote sensing data and field investigations for geological mapping and structural analysis. The case of SW Tichoukt ridge (Middle Atlas, Morocco), J. African Earth Sci., 198, https://doi.org/10.1016/j.jafrearsci.2022.104784, 2023.

Zeyen, H., Ayarza, P., Fernàndez, M., and Rimi, A.: Lithospheric structure under the western African-European plate boundary: A transect across the Atlas Mountains and the Gulf of Cadiz, Tectonics, 24, 1–16, https://doi.org/10.1029/2004TC001639, 2005.

Zhong, Y., Willett, S. D., Picotti, V., Xiong, J., and Zhang, H.: Spatial and Temporal Variations of Incision Rate of the Middle Yellow River and Its Tributaries, J. Geophys. Res. Earth Surf., 127, https://doi.org/10.1029/2021JF006327, 2022.

Zondervan, J. R., Stokes, M., Boulton, S. J., Telfer, M. W., and Mather, A. E.: Rock strength and structural controls on fluvial erodibility: Implications for drainage divide mobility in a collisional mountain belt, Earth Planet. Sci. Lett., 538, https://doi.org/10.1016/j.epsl.2020.116221, 2020a.

Zondervan, J. R., Stokes, M., Boulton, S. J., Telfer, M. W., and Mather, A. E.: Rock strength and structural controls on fluvial erodibility: Implications for drainage divide mobility in a collisional mountain belt, Earth Planet. Sci. Lett., 538, https://doi.org/10.1016/j.epsl.2020.116221, 2020b.

Zouhri, L., Lamouroux, C., Vachard, D., and Pique, A.: Evidence of flexural extension of the Rif foreland: The Rharb-Mamora basin (northern Morocco), Bull. la Société Géologique Fr., 173, 509–514, https://doi.org/10.2113/173.6.509, 2002.